EURAMET

FINAL PUBLISHABLE JRP REPORT

JRP-Contract number	SIB06
JRP short name	BioQuaRT
JRP full title	Biologically weighted quantities in radiotherapy
Version numbers of latest contracted Annex Ia and Annex Ib against which the assessment will be made	Annex Ia: V1.5 Annex Ib: V1.2
Period covered (dates)	From 01 June 2012 To 31 May 2015
JRP-Coordinator	
Name, title, organisation	Dr. Hans Rabus, head of department, PTB
Tel:	+495315926600
Email:	BioQuaRT@ptb.de
JRP website address	http://www.ptb.de/emrp/bioquart.html
Other JRP-Partners	ENEA, Italy
(Short name, country)	IRSN, France
	IST, Portugal
	NCBJ, Poland
	NPL, United Kingdom
	PoliMi, Italy

REG1-Researcher (associated Home Organisation):	Davide Moro, (INFN, Italy)	Start date: 01 Jun 2012 Duration: 36 months
REG2-Researcher (associated Home Organisation):	Jan Wilkens (MRI, Germany)	Start date: 01 Jun 2013 Duration: 24 months
REG3-Researcher (associated Home Organisation):	Ana Belchior (IST-ID, Portugal)	Start date: 01 Nov 2013 Duration: 18 months
ESRMG1-Researcher (associated Home Organisation):	Sabina Chiriotti Alvarez (SCK.CEN, Belgium)	Start date: 01 Nov 2013 Duration: 15 months
ESRMG2-Researcher (associated Home Organisation):	Marcin Pietrzak (NCBJ, Poland)	Start date: 01 Oct 2014 Duration: 5 months

Report Status: PU Public

SIB06 BioQuaRT

TABLE OF CONTENTS

1   Executive Summary

Introduction

Cancer treatment increasingly uses proton and ion beams, since they can deliver a similar dose to tumours as conventional x-ray based radiotherapy, but with less damage to surrounding healthy tissue. These new radiotherapy modalities need a new dosimetric concept to be established that would allow a clear separation of the physical and biological factors that contribute to the effectiveness of ionising radiation. The measurable physical properties of the track structure (the path that the beam takes through the DNA) and cell structures, depend on the particle type and energy. The biological factors are independent of radiotherapy modality, and reflect how the cells and DNA respond to the imparted energy. This project laid the foundations for a new concept of dosimetry for proton and ion beam radiotherapy and investigated establishing a multiscale model as the basis of the new quantities.

The Problem

In radiation oncology, new modalities have been emerging that offer therapeutic benefits, namely higher cure rates and fewer side effects from the treatment, but for which the planned dosage cannot be based on the physical quantity absorbed dose alone. So-called biological weighting factors have to be taken into account in the treatment planning. The determination of these weighting factors requires expensive radiobiological studies. In these studies, the biological outcome is generally investigated in relation to its dependence on the physical absorbed dose which is a macroscopic average quantity. However, the aforementioned biological weighting factors result from an entanglement of genuine biological effects, like the repair of radiation-induced damage to the genome, and physical factors, like the microscopic pattern of radiation interactions. Furthermore, different radiotherapy centres have been following different methodologies for determining the biological weighting factors. As a consequence, even when employing the same treatment modality, different centres may use up to a 20 % different physical dose for the same treatment situation. This has led to a detrimental confusion in interpreting clinical studies and it has hampered the exchange of information within the community.

The Solution

The aim of this project was therefore to establish a new dosimetric quantity which would allow a clear separation of the physical processes (dependent on the radiation modality) from the genuine micro-biological ones (independent of the radiation modality). To achieve this, measurement techniques for a comprehensive characterisation of the physical effects of the radiation were developed. This encompassed a characterisation of the radiation interaction pattern on length scales from the micrometre down to the nanometre, i.e. from the diameter of the cell nucleus down to the diameter of biological molecules inside the cells. Furthermore, cells experiments were conducted to investigate how this physical radiation interaction pattern correlates with the biological outcome of the irradiation.

Impact

The research undertaken by this project has significantly influenced the research priorities within European networks active in the field of ionizing radiation metrology. The results of the project enable the development of treatment planning tools for radiotherapy that are based on a so-called multi-scale approach and allow radiotherapy plans to be optimised not only in terms of physical dose, but also in terms of predicted treatment outcome.

In this way, clinical treatment plans from different centres can be compared and multi-centre studies on the clinical outcome of new modalities will become possible. In consequence, funding spent on such radio-oncology research will be utilised in an optimum way, so that fewer additional trials will be needed and the related health care expenses will be reduced in the long run. In particular, the project results may drastically reduce the need for expensive radiobiological cell experiments or animal experiments that were needed to establish the relative biological effectiveness of different treatments.

Aforementioned treatment planning tools will allow different radiotherapy modalities to be combined and it will provide radiotherapy researchers with improved capabilities for realising individualised radiotherapy. These tools will thus have a wide impact on clinical practice and will contribute to increased cure rates and better quality of life for the predicted 50 million European citizens that will be diagnosed with cancer and who will be treated with radiotherapy over the next two decades. The reduced side effects will also lead to a lowering of the overall cost to society of cancer treatments and post-treatment patient care.

2 Project context, rationale and objectives

<u>Context</u>

In radiotherapy, or the treatment of cancer using ionising radiation, the dosage is generally prescribed in terms of the physical quantity absorbed dose, which is defined as the absorbed radiation energy per unit mass. A number of new irradiation modalities, such as protons and carbon ions, have been emerging that offer therapeutic advantages over the conventionally used high-energy x-rays. When using these particle beams, it is known that a lower value of absorbed dose will lead to the same biological effect as conventional x-ray based radiotherapy, so this is taken into account by applying biological weighting factors in the treatment planning.

These biological weighting factors are generally determined by performing expensive radiobiological tests at the radiotherapy centres, but there is variability between centres and methodologies. It is generally agreed that the diversity of methods being used to derive biological weighting factors leads to confusion in interpretation and ultimately possible risk to patients. A universally agreed approach for the weighting factors would facilitate exchange of information and improve collaboration between centres and within the radiation oncology community.

The biological weighting factors to convert an absorbed dose to a biological effective dose depend upon the physical interactions of the radiation with tissue and the biological response of the cells in the organism. The metrological challenge was to establish a new dosimetric quantity which would allow a transparent separation of the physical processes (dependent on radiotherapy modality) from the genuine biological ones (independent of modality). The Consultative Committee of Ionising Radiation (CCRI) of the Meter Convention has expressed strong support for defining such a new quantity, particularly for treatments involving the use of several multiplying factors to describe the corresponding biological effects of the absorbed dose.

Given the complexity of the initiation and occurrence of biological processes on various time and length scales, neither microdosimetry nor nanodosimetry on their own can fully describe the biological process occurring over time and distance. Therefore, a multiscale approach, which aims to combine the effects at the cell level (microdosimetry) and with the interaction at the DNA scale (nanodosimetry), is needed to get a full understanding of the effects. This will mean that the radiation can have maximum benefit with minimum damage to surrounding tissue.

<u>Objectives</u>

The first two objectives addressed the way the radiation penetrated the tissue at the cellular and DNA scales, using different types of radiation detectors to mimic tissue.

- To develop micro-calorimeters directly measuring energy deposition spectra and to compare them with tissue-equivalent proportional counters and silicon based microdosimeters.

- To develop improved techniques for measuring ionising-particle track structure and its characteristics with nanometre resolution.

The third objective looked at the chemical reactions caused by the interaction between the radiation and the DNA.

- To develop methods for measuring the production rate and 3D distribution of reactive oxygen species in tissue exposed to proton and ion beams as a function of particle type and energy.

The fourth and fifth objective looked at simulation and modelling of radiation delivery and its effects on the body.

- To develop a numerical tool (based on DNA ionisation and fragmentation cross sections) for the multi-scale simulation of ionising particle track structure and biological effects of ionising radiation.

- To develop quantitative models to link the physical quantities with the biological outcome and to determine free parameters in the multi-scale model from biological assays.

3   Research results

Objective 1: To develop micro-calorimeters directly measuring energy deposition spectra and to compare them with tissue-equivalent proportional counters and silicon based microdosimeters.

The purpose of this work was to develop a set of micro-calorimeters, with dimensions at the scale of a cell or cell nucleus, to provide a means of directly measuring the energy and energy spectra deposited by ionizing radiation. The goal was to carry out a comparison of this new detector with existing microdosimeters, the mini-tissue equivalent proportional counter (mini-TEPC) and the Si-micro-telescope. Due to the complications explained below it was not possible to carry out the comparison of the three detectors within the time frame of the project but significant progress was made towards this goal.

Nevertheless, from the work performed during the BioQuaRT project, several conclusions arose: Whilst the micro-calorimeters developed by NPL promise significant advantages over existing devices, particularly by providing a direct measure of energy and for the improved energy resolution possible the project remains challenging. Much has been learnt over the course of the project but there is still work to be done before a working device is completely realised. It is hoped that the knowledge gained during this project can be used to inform the next stage of development.

The computational simulations carried out in this work by NPL, IST, PoliMi and IRSN serve to demonstrate how significant insight can be gained about an experiment or a detector through the use of Monte Carlo and Finite Element Analysis. The work here also demonstrates that even for demanding applications such as microdosimetry both the Geometry and Tracking 4 (Geant4) and Monte Carlo N-Particle (MCNP) Monte Carlo packages can reproduce experimental results with good agreement. The Monte Carlo simulations of the Si-micro-telescope detector by NPL, PoliMi and IST, combined with experimental measurements carried out by PoliMi at the Surrey Ion Beam Centre, highlighted the need for a correction factor to correct for the low energy events measured.

In order to be able to compare the results obtained with the three different types of microdosimetric device, i.e. micro-calorimeter, mini-TEPC and Si-micro-telescope, an experimental setup which allows the repeatable positioning of each device during one experimental run was required. It was also necessary to provide a means of shifting the effective depth of the measurements so as to measure the spectra at a range of positions along the depth dose curve. To achieve this, an experimental setup was designed by REG(INFN), built by NPL and later tested by PoliMi and REG(INFN) at the Catania beam line using the mini-TEPC and the Si-micro-telescope detectors.

Here after, we give a brief description of the results achieved:

The micro-calorimeters

The development of the micro-calorimeters was carried out by NPL. A micro-calorimeter consists of a loop of superconductor surrounding, but electrically isolated from, a second film of superconductor located within this loop. The loop of superconductor is interrupted by two weak link, or Josephson, junctions creating a Superconducting Quantum Interference Device (SQUID), a device which is extremely sensitive to magnetic fields passing through the loop. An example of a micro-calorimeter is given in Figure 1.1.

During operation incident radiation causes heating within the superconducting absorber located within the SQUID. This heating causes a change in the penetration length, the depth to which magnetic fields can penetrate the absorber, which is detected by the SQUID as a voltage change.
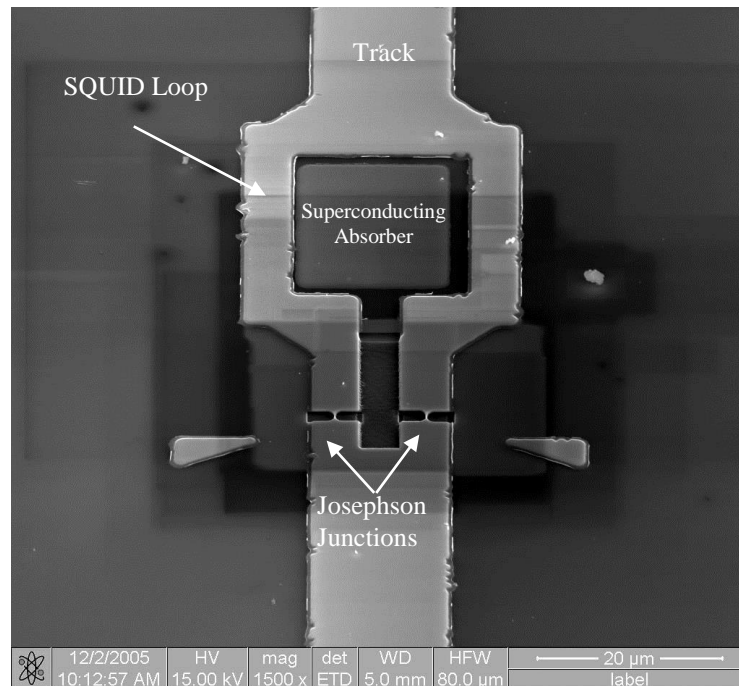
Figure 1.1: *SEM Image of original SQUID Design.*

Computational Modelling

As part of this project detailed Monte Carlo radiation transport simulations were carried out using the Geant4 Monte Carlo toolkit (low energy standard and Geant4-DNA (deoxyribonucleic acid) processes) and the Monte Carlo N-Particle eXtended (MCNPX). The simulations using the standard Geant4 toolkit were performed by NPL and those using MCNPX were performed by IST. IRSN conducted the simulations using the Geant4-DNA code. These simulations were used to determine the expected microdosimetric spectra of the micro-calorimeters as well as providing a means of comparing the response of each code. The results of the comparison show that Geant4 and Geant4-DNA give very similar results whilst the MCNPX results show a discontinuity at around 100 keV/μm, which is probably due to the higher energy cut-off value in electron transport in MCNPX. The Monte Carlo results were also used as an input into a Finite Element Analysis model of heat transfer. This was used to investigate the thermal response of the device as well as the contamination of the signal due to energy deposited directly from the incident radiation in the superconducting and substrate layers. This model confirmed that the expected response time of a device to a single incident event is of the order of a nanosecond. The effect of energy deposited directly in the superconducting layer is not trivial and so ideally in future designs an alternative material with a high transition temperature yet lower thickness should be used.

Additional simulations of the mini-TEPC and Si-micro-telescope detectors were also carried out using the Geant4 toolkit and the then newly released MCNP6 code. The results for the Si-micro-telescope simulations gave agreements between the codes of between 6 % and 17 % and of between 5 % and 17 % between simulation and experiment. The experimental results showed an unexpected contribution from low lineal energy events as shown in Figure 1.2 leading to a correction factor to account for these low energy events.
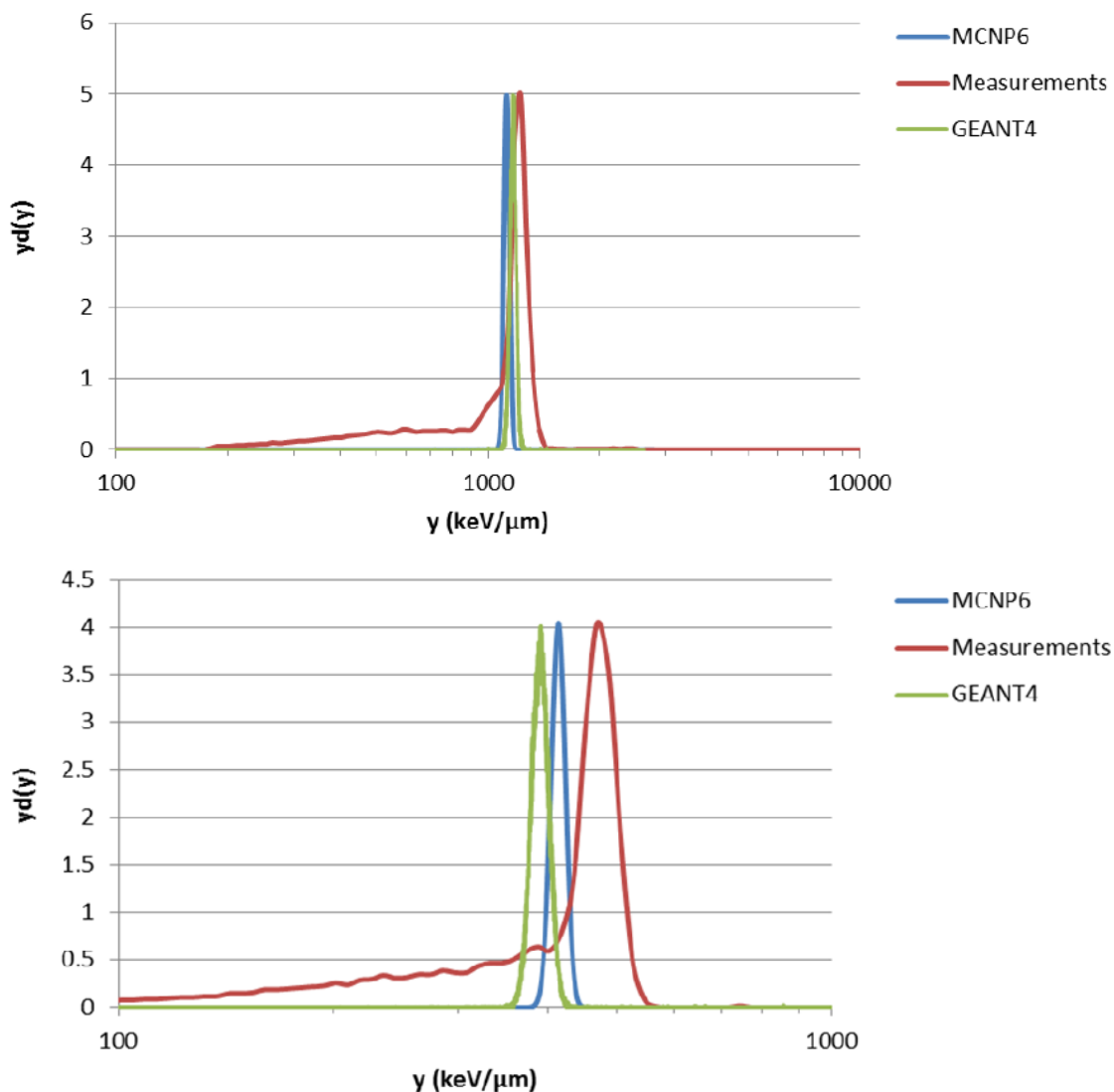
Figure 1.2*: Experimental vs. Monte Carlo energy deposition spectra for the Si-micro-telescope. Upper panel: 9.96 MeV carbon ions, lower panel: 4.5 MeV lithium ions.*

For the mini-TEPC the agreement is qualitatively good with Geant4 results providing a generally good shape and peak energy agreement. The MCNP6 results also show a good agreement in the shape and shape change although some unexpected contributions from higher energy events are apparent which do not appear in the experimental or Geant4 results.

Development of the devices

During this project a series of micro-calorimeters were created by NPL according to the design outline given above. In order to use each device the characteristic parameters need to be determined. These include the superconducting transition temperature, the junction critical current and the magnetic bias required for each device. For these devices the transition temperatures were found to be 5.9 – 6.5 K, the critical currents vary with temperature from 5 µA to 150 µA. The coil currents generating the magnetic bias are specific for each device but are typically 0-5 µA. Used together these parameters allow the devices to be operated.

The devices were then irradiated with a range of beams to investigate the response of the SQUID loop under different conditions. These measurements included radiation hardness measurements of the devices with the microbeam at the Surrey Ion Beam Centre using a proton beam to establish whether the devices would survive prolonged exposure. Dose rates as high as 100,000 times that expected to be required for routine measurements were used and the devices showed no signs of altered properties. The devices were also exposed to beams of alpha particles using a Polonium-210 source and again no noticeable changes to the devices' characteristics were measured. Measurements were also carried out using ^{60}Co gamma-rays to establish the threshold dose rate for which the devices could be used under broad beam conditions. This is important as the operational parameters of the devices depend on temperature and in a clinical setting it would be extremely challenging to shield the SQUID loop during measurements. During these measurements it was found that the devices can be used under broad beam conditions provided that the dose rate is below about 0.011 cGy/s for ^{60}Co gamma-rays.

Due to the nature of working with superconductors of small dimensions, difficulties are likely to be encountered and this project has been no exception. One major difficulty encountered was with the superconducting absorber being too thin and thus not having the desired superconducting properties. Considerable effort has been spent during this project to overcome this limitation, details of which are provided here. Unfortunately, the original supplier was not able to produce an alternative batch of devices as their production machine was no longer in operation and so a work-around was required. To do this an alternative superconductor was deposited on top of the original in layers approximately 500 nm thick. This material, tungsten based, has been shown in previous measurements to have superconducting properties at close to 5 K which is relatively close to the transition temperature of the Niobium superconductor originally intended. Various measurements were carried out to measure the transition temperature of this new superconducting absorber and it was ultimately determined to be between 4.6 and 5.1 K (the range being due to purity and thickness variations). In order to operate the SQUID device at this temperature the transition temperature of the junctions needed to be suppressed to enable operation within the range of the absorber transition. This was achieved by thinning the junctions. Unfortunately, this carried the side effect of causing the devices to become highly sensitive to damage rendering the device inoperable.

Improved devices

Using the information gained from the prototype devices two types of improved device were designed by NPL. These devices have the same SQUID loop design as the prototypes but have new superconducting absorber materials. These materials have much higher transition temperatures which were verified by the supplier but also have thicknesses of the order of a few nanometres. This provides a significant improvement on the contribution of energy deposited directly into the superconducting absorber from ionizing radiation as investigated in the thermal modelling of the prototype devices.

As these devices work on the same operational principles as the original devices, only varying by their dimensions, the same characterisation measurements were carried out to establish the optimum operational parameters. As these devices were produced by a different supplier the quality of the superconducting film was different. This means that the superconducting transition of junctions of the devices are much sharper (occurring over < 0.025 K as compared to about 0.15 K for the prototype devices). This means that the devices are highly sensitive to the thermal stability of the sample stage and so the devices typically take over 30 minutes to settle between measurements.

During irradiations in a clinical beam the entire device would be subject to incident radiation and so it is important to determine how the device responds under such conditions. To do this the devices were tested in a Cobalt-60 beam. It was found that under broad beam conditions the parameters required to operate the device would change with dose rates above about 30 µGy/s.

Experimental setup designed and built for the inter-comparison

In order to be able to compare the three detectors in a single experiment a special experimental rig was required. This rig was designed by REG (INFN) with input from NPL and PoliMi to allow switching between the devices during a single experimental run whilst maintaining accurate positioning of the detectors after the initial setup. The positioning was achieved by providing a means of fixing the rig to the beam line as well as through the use of linear stages to move the mini-TEPC and Si-micro-telescope in and out of the beam. Due to the cryogenic temperatures required for the micro-calorimeters the cryostat containing these detectors would be mounted behind the other detectors. In addition to the positioning, the rig provides a simple means of adjusting the equivalent depth along the depth dose curve without affecting the setup of the detectors. This was achieved by using a block of poly(methylmethacrylate) (PMMA) containing PMMA discs of different thickness to provide range shifts along the depth dose curve. A sketch of the design and the final rig that was built is shown in Figure 1.4 and a photograph of it in use at the Catania beam line is given in Figure 1.5.
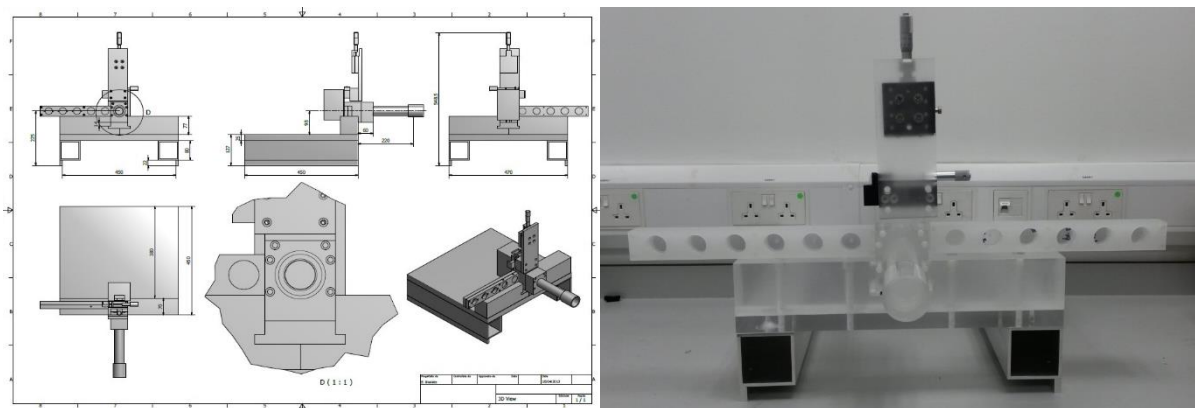

Figure 1.4: Experimental set up rig for comparison.

Figure 1.5: Experimental rig in use at the Catania beam line.

Comparison of mini-TEPC and Si-micro-telescope

Exploiting the set-up described in the previous section, a microdosimetric characterisation of a clinical carbon-ion beam was carried out employing a miniTEPC and a Si-microtelescope as developed by REG(INFN) and PoliMi, respectively. As the two devices were used in the same experimental set-up, the measurement results could be directly compared.

The measurements were performed by REG(INFN) and PoliMi together with ESRMG(SCK.CEN) at the Italian National Centre of Oncological Hadrontherapy (CNAO) using an initially monoenergetic carbon ion beam with energy 195.2 MeV/u, equivalent to the 80 mm range in water. Due to the narrowness of the energy distribution of the primary beam, two ripple filters (passive energy modulators) were used to spread it in order to simplify investigation of the Bragg peak region. The active scanning treatment facility was used to uniformly irradiate a target area of 3×3 cm^2 by scanning this area with 225 spots of about 1 cm in diameter each and by repeating this procedure 10 times. Figure 1.6 shows the CNAO treatment room and the experimental set-up.
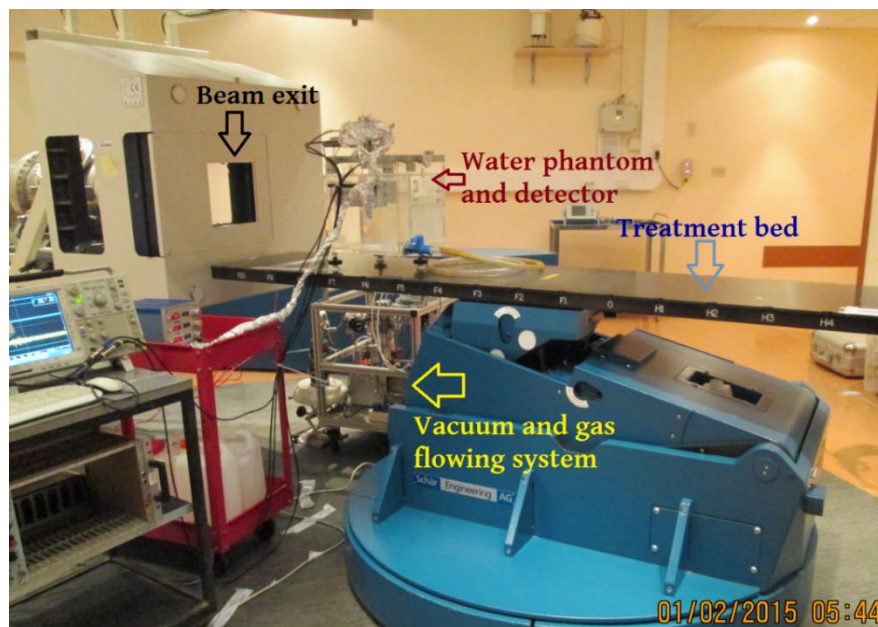

Figure 1.6. *Experimental set-up adopted for the microdosimetric characterisation at CNAO.*

The two microdosimeters used for the measurements were deliberately developed to operate in a pulsed and actively-scanned beam of carbon ions. A new mini TEPC was properly designed and constructed by REG(INFN) with the aim to reduce the spectral distortions observed at very high lineal energy values. Before being used to perform microdosimetric measurements at CNAO, the new mini TEPC was tested with photon and fast neutron beams by REG(INFN) and ESRMG(SCK.CEN) at the INFN Legnaro national laboratory. Test measurements were performed by filling the detector with pure propane gas at about 450 mbar of pressure. At such a pressure, the ionization yield inside the cylindrical 0.9 mm cavity matches that of a 0.1 mg/cm^2 site filled with a tissue equivalent gas mixture based on propane or a site of 1 µm in tissue. The mini TEPC was finally inserted in a tiny aluminium stem and placed in a cylindrical plastic holder (made of polymethylmethacrylate) which allowed it to be positioned at the centre of the water phantom adopted for the characterisation at CNAO.

A solid-state microdosimeter based on a monolithic silicon telescope was also especially designed and developed by PoliMi to measure in the same experimental set-up adopted for the mini-TEPC. The silicon detector consisted of a surface ΔE stage, about 2 µm in thickness, geometrically segmented in micrometric cylinders of 9 µm in diameter, coupled to a single deep E stage of about 500 µm in

thickness. The Δ*E-E* structure had been previously demonstrated to measure microdosimetric spectra through an optimised event-by-event tissue equivalent correction. The system was designed in order to operate in the water phantom selected at CNAO at a distance of about 30 cm from the front-end electronics. A dedicated plastic holder was fabricated to host the detector and to position it along the carbon beam axis.

The microdosimetric spectra collected through the two systems are shown in Figure 1.7. Those distributions measured at positions before the Bragg peak show almost Gaussian shapes since in this region the absorbed dose is largely due to fast carbon ions. Spectra collected on the distal edge of the Bragg peak show a shift of the main peak toward the carbon-edge value of 1397 keV/μm. This behaviour corresponds to the fact that, by increasing the depth, the absorbed dose is more and more due to low energy carbon ions, the maximum stopping power of which is 931 keV/μm in liquid water.
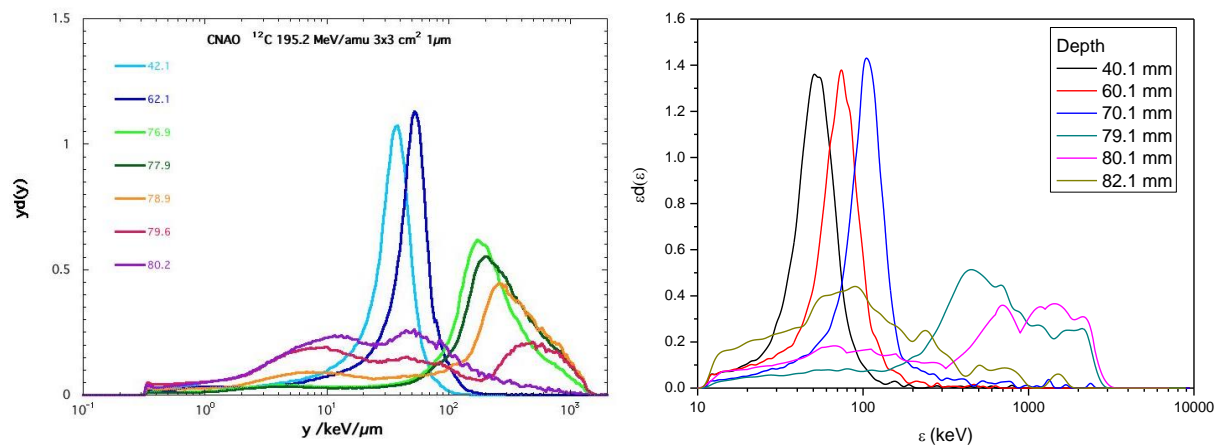
Figure 1.7. *Microdosimetric spectra of lineal energy y measured at different depths in a water phantom by the mini-TEPC (left) and the silicon micro-telescope (right).*

Beyond the distal edge, at larger values of depth inside the phantom, events at smaller lineal energy values (less than 100 keV/μm) play a major role in the delivery of absorbed dose. Monte Carlo calculations performed by ESRMG(SCK.CEN) suggest that those events are due to protons and helium ions, while the peak at bigger y-values is due to helium and boron ions.

Figure 1.8 reports the direct comparison of lineal energy distributions measured by the two detection systems used at 40.2 mm and 60.2 mm in water. As can be observed, despite the difference in the detection threshold, which is higher for the Si-microdosimeter, the agreement between the spectra is satisfactory.
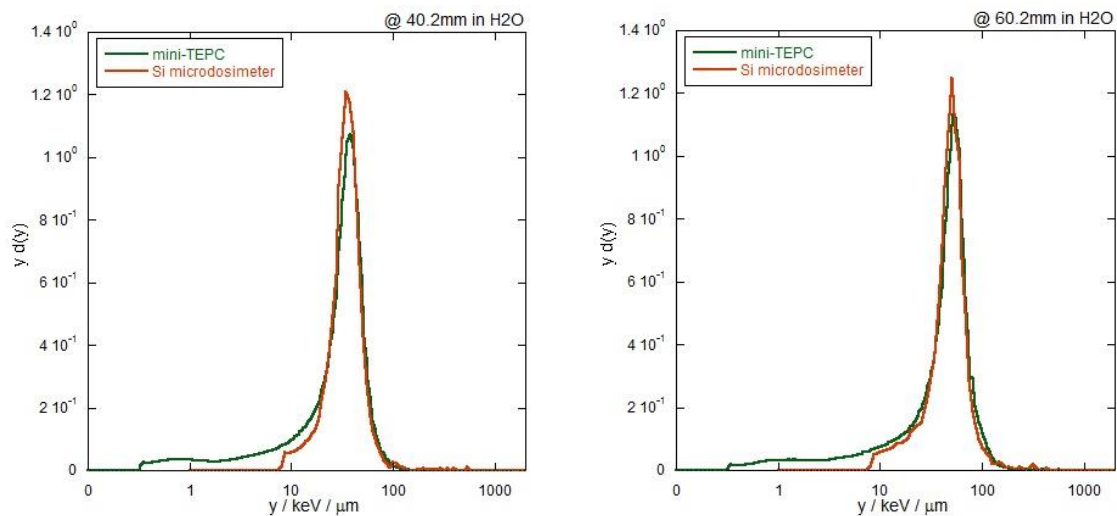
Figure 1.8. *Comparison between the lineal energy distribution measured by the Si-microdosimeter and the mini-TEPC at two different depths in a water phantom.*

Objective 2: To develop improved techniques for measuring ionizing-particle track structure and its characteristics with nanometre resolution.

The upgrade of the PTB Ion Counter by integrating the PoLiMi Si-micro-telescope gave rise to an innovative device capable of measuring nanodosimetric and microdosimetric track structure characteristics of the same radiation quality in the same measurement run. This type of measurement could not be carried out before and it enables the nanodosimetric and microdosimetric track structure characteristics of the respective radiation quality to be correlated.

Up to now the only target gases used in nanodosimetric track structure measurements have been nitrogen and propane. In order to obtain track structure information as close as possible to the experimental situation of the cell exposures (see objective 5), water vapour gas targets and gas targets representing DNA constituents consisting of tetrahydrofurane (THF) and pyrimidine were prepared successfully for the first time in the PTB Ion Counter. Track structure measurements were carried out using these gas targets. However, because pyrimidine significantly and rapidly degrades the performance of the secondary electron multiplier, there is no long term experience with gas targets prepared from pyrimidine at present.

With respect to experimental nanodosimetry, an aspect of fundamental importance is the consistency of the measurements of nanodosimetric quantities describing track structure characteristics. Therefore, an intercomparison between the three nanodosimeters involved in the project was carried out. As two of the three devices (INFN StarTrack Counter and NCBJ Jet Counter) were stationary setups, the PTB Ion Counter was used as a comparison device and it was transported to the location of the two other nanodosimeters to run measurements in almost the same radiation fields. Although the three devices involved in the project differ substantially in several aspects regarding their operation and detection schemes, the intercomparison of the nanodosimeters led to consistent ionization cluster size distributions, as is described in the two paragraphs dealing with the pairwise comparisons of the nanodosimeters.

Moreover, the intercomparison gave rise to a real novelty in our knowledge of radiation interaction in nanometric volumes. In spite of the differences among the three nanodosimeters, the data obtained with the three nanodosimeters are found to be located on the same curve, when plotting the cumulative sum F_k of the cluster size distributions for cluster sizes $v \geq k$ as a function of the mean ionization cluster size M_1. On the one hand this finding proves the consistency among the

measurements obtained with the three nanodosimeters, and on the other hand it gives evidence to the existence of a set of functions $F_k(M_1)$ being invariant with respect to both, the radiation quality of the primary ion (mass, charge and velocity) and the target properties (gas type, pressure and size), but only depending on the mean ionization cluster size M_1. Therefore, this set of functions $F_k(M_1)$ together with M_1 might serve as a qualifier to describe the "nanodosimetric" radiation quality of a radiation field.

Combining nanodosimetry (PTB Ion Counter) and microdosimetry (PoLiMi Si-micro-telescope)

PoLiMi developed a microdosimetric detector based on silicon as the detector material. The design of this detector is that of a telescope. This Si-micro-telescope basically consists of a stack of two individual detectors embedded into the same substrate: a thin layer of silicon absorbing only a small fraction of the primary particle's energy and thus acting as an energy loss spectrometer, and a thick layer of silicon located beyond the thin layer absorbing the remaining energy of the primary particle.

In order to carry out measurements providing both nanodosimetric and microdosimetric information in the same measurement run, the Si-micro-telescope was integrated into the Ion Counter. Using the summed signal of the two detecting layers as a trigger signal allowed the measurement of ionization cluster size distributions, which is a nanodosimetric quantity. In addition, the sum signal of the two detectors yields the energy of the primary particle. The signal of the thin detector stage provides information on microdosimetric quantities, thus the integration of the Si-micro-telescope into the Ion Counter allows combined micro- and nanodosimetric measurements.

Figure 2.1 shows the measurements with the Si-micro-telescope integrated into the PTB Ion Counter. The measurements were carried out at the accelerator facilities of the PTB with protons (left) and alpha particles (right) in the range between 0.26 MeV and 2.5 MeV, using 1.2 mbar C_3H_8 as the target gas. The data show the energy deposition (pulse height) in the thin detector layer, denoted as ΔE-stage, and the thick detector layer, denoted as E-stage, together with the first moment of the ionization cluster size distribution, that is the mean ionization cluster size M_1.
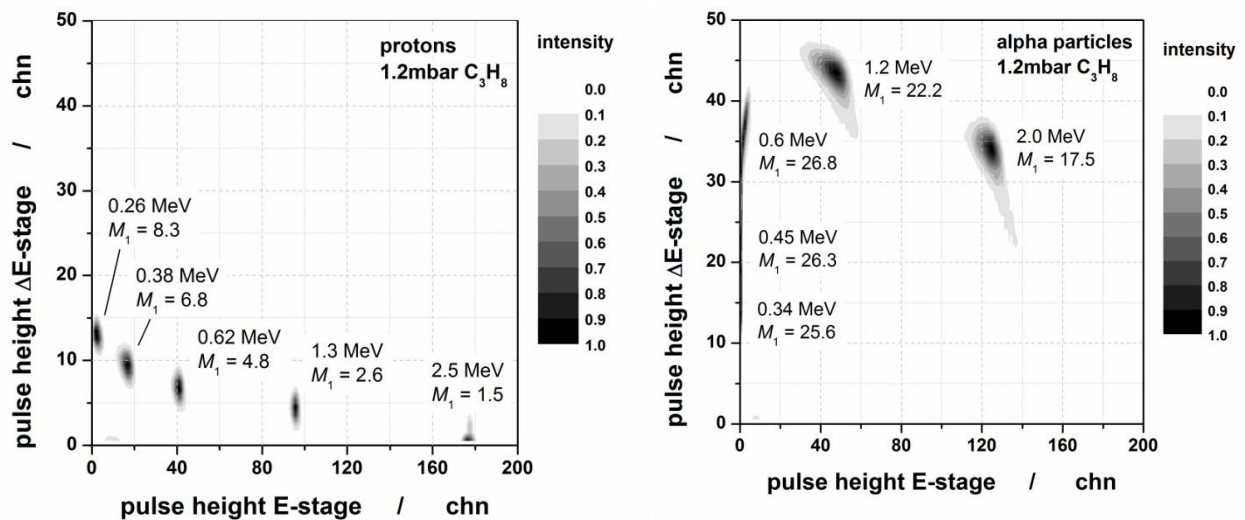
Figure 2.1: *Combined nanodosimetric and microdosimetric measurements with protons (left) and alpha particles (right) in 1.2 mbar C_3H_8.*

In the figure above showing the proton measurements (left), it can be seen that with increasing proton energy, the pulse height of the ΔE-stage, which represents the energy deposited in the ΔE-stage and thus corresponds to the energy loss of the protons when passing through the ΔE-stage, decreases with increasing proton energy due to the decreasing linear energy transfer (LET). Simultaneously, the pulse height of the E-stage, which corresponds to the remaining energy of the proton after its passage through the ΔE-stage, increases with increasing proton energy. Since the Bragg peak energy for protons in C_3H_8 is at 65 keV, the mean ionization cluster size M_1 decreases with decreasing LET due to the increasing proton energy.

The measurements for alpha particles (right) show a different behaviour. For alpha particles of very low energy (i.e. 0.34 MeV – 0.6 MeV) only the energy loss (i.e. the pulse height) of the alpha particle passing through the ΔE-stage increases, whereas the energy deposited in the E-stage is almost zero. The reason is that the range of alpha particles of such low energy is smaller than the thickness of the ΔE-stage and therefore the whole particle energy is deposited in this stage. Additionally, it can be seen, that the mean ionization cluster size M_1 increases with the increasing LET of the alpha particles, since the Bragg peak energy for alpha particles in C_3H_8 is at 550 keV. For alpha particles having a range exceeding the thickness of the ΔE-stage, a behaviour similar to that previously obtained for protons is found: with increasing alpha particle energy the energy loss of the alpha particle passing through the ΔE-stage decreases due to the decreasing LET of the alpha particles, whereas the energy deposited in the E-stage increases with increasing alpha particle energy, and the mean ionization cluster size M_1 decreases with decreasing LET due to the increasing alpha particle energy.

Track structure measurements in a gas target of DNA constituents and water vapour (PTB Ion Counter)

To obtain track structure information as close as possible to the experimental situation of the cell exposures for objective 5, track structure measurements with the PTB Ion Counter using gas targets consisting of molecules representing DNA constituents and water vapour were planned to be carried out. Gas targets of water vapour and gas targets of tetrahydrofurane (THF) and pyrimidine representing DNA constituents were prepared successfully. The measurements were carried out at the PTB ion accelerator facilities using protons and alpha particles in the energy range between 0.15 MeV and 20 MeV. In the measurements, the primary particle passes the target volume centrally.

Figure 2.2 shows the mean ionization cluster sizes M_1 measured with protons (left) and alpha particles (right) as a function of the primary particle energy for the two target gases (THF and water vapour). Independent from the target gas, the mean ionization cluster sizes show an identical behaviour for the two different types of primary particles: for protons, the mean ionization cluster size decreases with increasing energy, whereas for alpha particles, M_1 at first increases up to the Bragg peak energy and then towards higher energy also decreases with increasing alpha particle energy. However, for both protons and alpha particles, the mean ionization cluster size differs by a factor of about 8 for the two target gases, reflecting the difference in the cross sections.
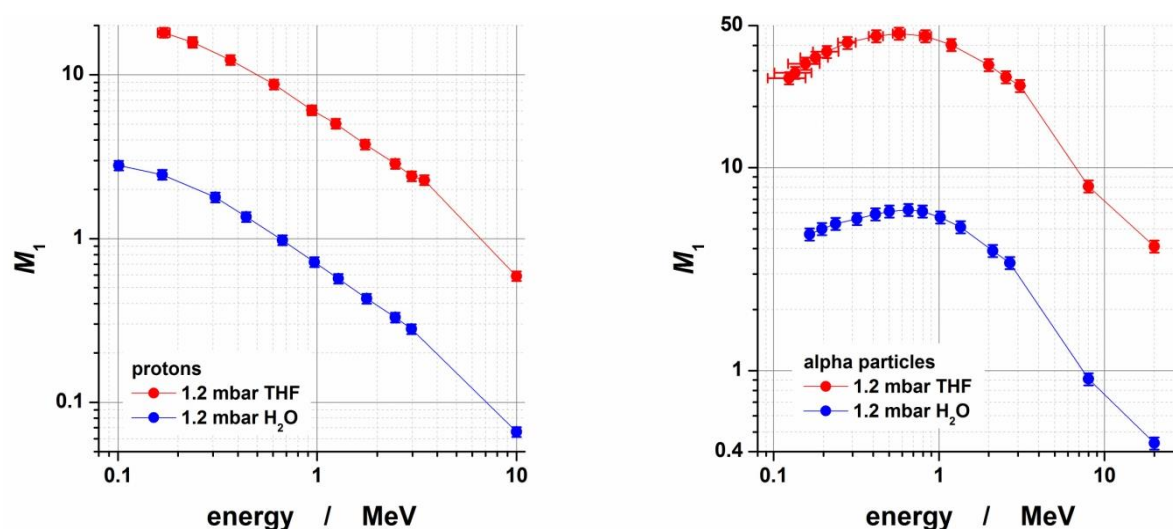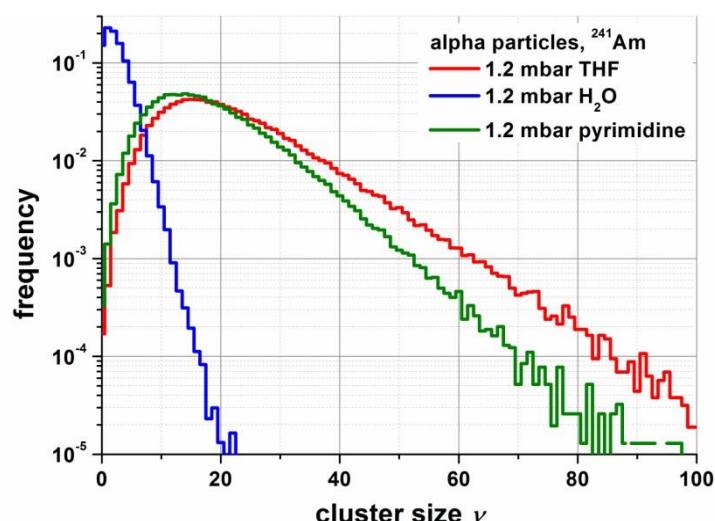

Figure 2.2: Mean ionization cluster sizes M_1 measured with protons (left) and alpha particles (right) in 1.2 mbar THF and in 1.2 mbar H_2O (water vapour).

In Figure 2.3, ionization cluster size distributions measured with alpha particles from a [241]Am-source in THF, water vapour and pyrimidine at a gas pressure of 1.2 mbar are shown. The direct comparison of the cluster size distributions obtained for the same radiation quality confirms the difference in the

mean cluster size between THF and water vapour of the same target pressure: the maximum of the cluster size distribution is located at a much larger cluster size for THF than for water vapour, and the size of the ionization clusters found at the same level of occurrence is much larger for THF than for water vapour. In contrast, the difference of the cluster size distributions of THF and pyrimidine is much less pronounced, indicating that the cross sections for ionization are rather close by for these two target gases.
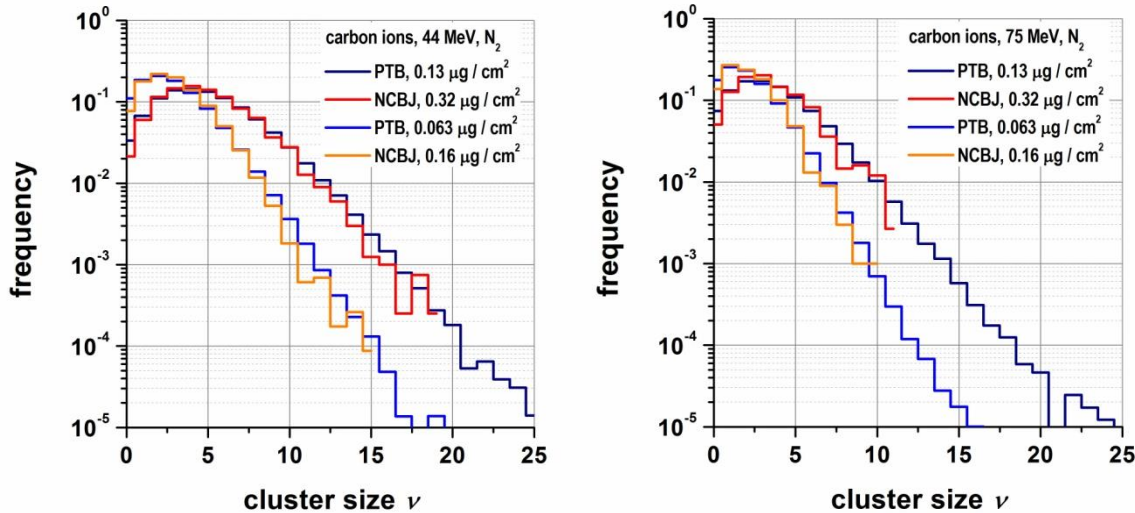

Figure 2.3: *Ionization cluster size distributions measured with alpha particles from a ^{241}Am-source in THF, water vapour and pyrimidine at a gas pressure of 1.2 mbar.*

However, at present, there is no long term experience with gas target prepared from pyrimidine, since it was only prepared a few times, because it seems, that pyrimidine significantly and rapidly degrades the performance of the secondary electron multiplier, which is used for the detection of the ionized gas molecules in the Ion Counter's sensitive volume. Therefore, no further measurements with pyrimidine were carried out with the PTB Ion Counter.

Comparing different nanodosimeters: NCBJ Jet Counter and PTB Ion Counter

Two different nanodosimeters, the NCBJ Jet Counter and the PTB Ion Counter, both capable of measuring the ionization track structure of carbon ions in a gas target equivalent to a nanometric site in a condensed matter, were compared with respect to the cluster size distribution measured with these two devices. The measurements were carried out at the accelerator facility at the Heavy Ion Laboratory (HIL) of the University of Warsaw. In both nanodosimeters, the target gas was nitrogen. The nanometric sites used in the two devices were selected such, that the difference in mass density in the target volume compensates for the differences of the ion counting efficiencies η of the two devices. The ratio of the counting efficiencies of the two nanodosimeters was found to be $\eta_{NCBJ\text{-}JC} / \eta_{PTB\text{-}IC} \cong 0.4$. Therefore, the mass density in the target volumes used in the two devices for the comparison were adjusted such, that their ratio reflects the ratio of the counting efficiencies. Thus, the mass density in the target volume of 0.063 µg/cm^2 of the PTB Ion Counter was matched to a mass density of 0.16 µg/cm^2 of the NCBJ Jet Counter. The approximately same ratio of the mass densities was attained for a mass density of 0.13 µg/cm^2 of the PTB Ion Counter and for a mass density of 0.32 µg/cm^2 of the NCBJ Jet Counter. The ionization cluster size distributions produced by one single carbon ion for a central passage in the above mentioned nanometric sites were measured for the two primary carbon energies, 44 MeV and 75 MeV. The comparison of the resulting ionization cluster size distributions (see Figure 2.4) for both pairs of mass densities in the target volume show that the effect of the ion counting efficiency can be compensated for by proper adjustment of the mass density in the target volume, supporting the concept of an "effective size", which takes into account the mass contained in the sensitive volume combined with the counting efficiency. These results mean that both

devices, the PTB Ion Counter and the NCBJ Jet Counter, yield equivalent results at least for central passage of carbon ions through the measured volumes.

Figure 2.4: *Comparison of the ionization cluster size distributions measured with the NCBJ Jet Counter and the PTB Ion Counter for 44 MeV (left) and 76 MeV (right) carbon ions for mass densities in the target volume of the NCBJ Jet Counter of 0.16 µg/cm² and 0.32 µg/cm² and for mass densities of 0.063 µg/cm² and 0.13 µg/cm² in the PTB Ion Counter, respectively. The ratio of the mass densities in the target volume of the two nanodosimeters takes into account the ratio of the counting efficiencies η of the two nanodosimeters $\eta_{NCBJ-JC} / \eta_{PTB-IC} \cong 0.4$.*

While the shape of the ionization cluster size distributions can be matched at large by using density scaling, Figure 2.4 also indicates that discrepancies persist for large cluster sizes. Therefore, the comparison of the PTB Ion Counter and the NCBJ Jet Counter shown in Figure 2.4 was complemented with research undertaken by ESRMG(NCBJ) who developed a dedicated Monte Carlo simulation based on the Geant4-DNA simulation toolkit. The new simulation takes into account experimental details such as the existence of a mylar wall around the sensitive volume in the Jet Counter and the non-uniform collection efficiency in the Ion Counter. The simulations showed that the differences in the shape of ionization cluster-size distributions should be negligible compared to the measurement uncertainties. ESRMG(NCBJ) also investigated experimentally the dependence of the mean cluster size and the shape of the ICSD on the accelerating voltage applied in the Ion Counter. The results also ruled out the accelerating voltage as a cause of the differences at large cluster sizes.

Comparing different nanodosimeters: REG(INFN) StarTrack Counter and PTB Ion Counter

The two devices are both able to count the number of ionizations produced by single ions within a target volume with the primary ion crossing or passing the target volume at a specified distance. The devices differ in several aspects: (i) the StarTrack Counter is based on single electron counting technique whereas the Ion Counter is based on single ion counting, (ii) the target volumes have cylindrical shape in both cases, but the physical dimensions are different as well as the gas density and (iii) the counting efficiencies are different.

Measurements with carbon ions at 150 MeV and 96 MeV were carried out at the Tandem-Alpi accelerator complex of the INFN - Legnaro National Laboratories, at different impact parameters d, which is the distance between the primary ion trajectory with respect to the centre of the target volume. In the case of the StarTrack Counter the impact parameter d was changed between 0 mm and 8 mm which corresponds to a maximum distance in terms of mass per area of about 4.1 µg/cm². In the measurements with the Ion Counter, the impact parameter d varied between 0 mm and 7.7 mm,

which corresponds to a maximum distance in terms of mass per area mass per area of about 1.7 µg/cm^2. In both devices the target gas was C_3H_8 at a gas pressure of 3 mbar in the StarTrack Counter and 1.2 mbar in the Ion Counter.

The investigation of the track structure properties was extended to the penumbra region of particle tracks, i.e. for primary trajectories passing outside the target volume. As an example, Figure 2.5 show some cluster size distributions in the penumbra region of 150 MeV carbon ions, measured with the StarTrack Counter (left) and with the Ion Counter (right), respectively. As already observed in previous investigations[1,2], the shape of the cluster distributions for $\nu > 0$ is almost independent of the impact parameter d. The probability of zero ionizations $P_0(Q,d)$ increases with increasing impact parameter d, mainly due to the decrease of the solid angle.
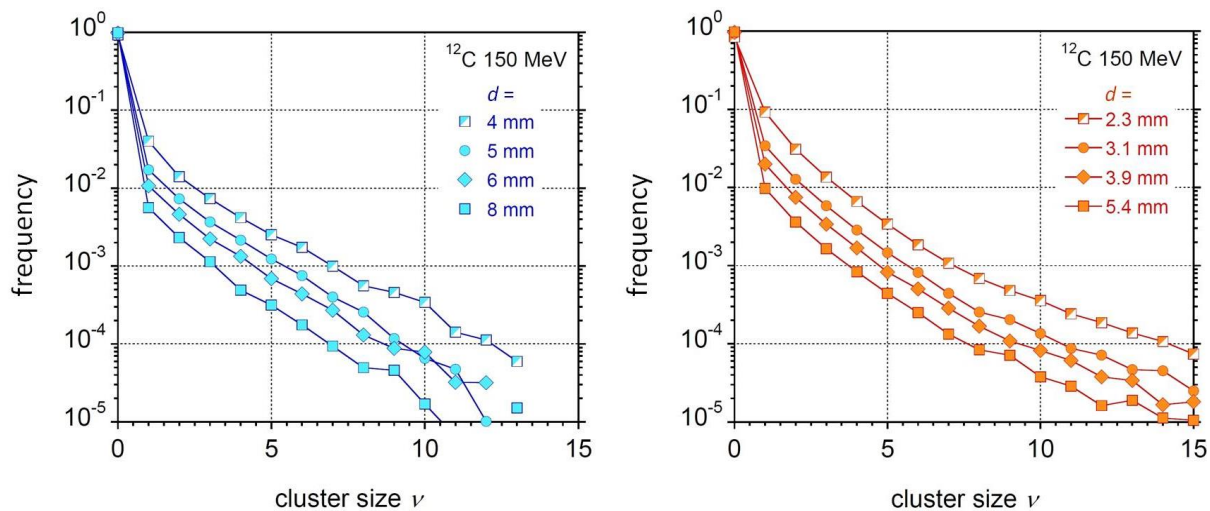
Figure 2.5: *Cluster size distributions measured with the StarTrack Counter (left) and the Ion Counter (right) in the penumbra region of 150 MeV carbon ions.*

Similar results were obtained for the 96 MeV carbon ions. Apart from the frequency for cluster size $\nu = 0$, the shape of the cluster size distributions in the penumbra region of particle tracks is almost independent from the impact parameter and also from radiation quality.

---

[1] V. Bashkirov et al., Rad. Prot. Dosim. 122, 415-419 (2006)
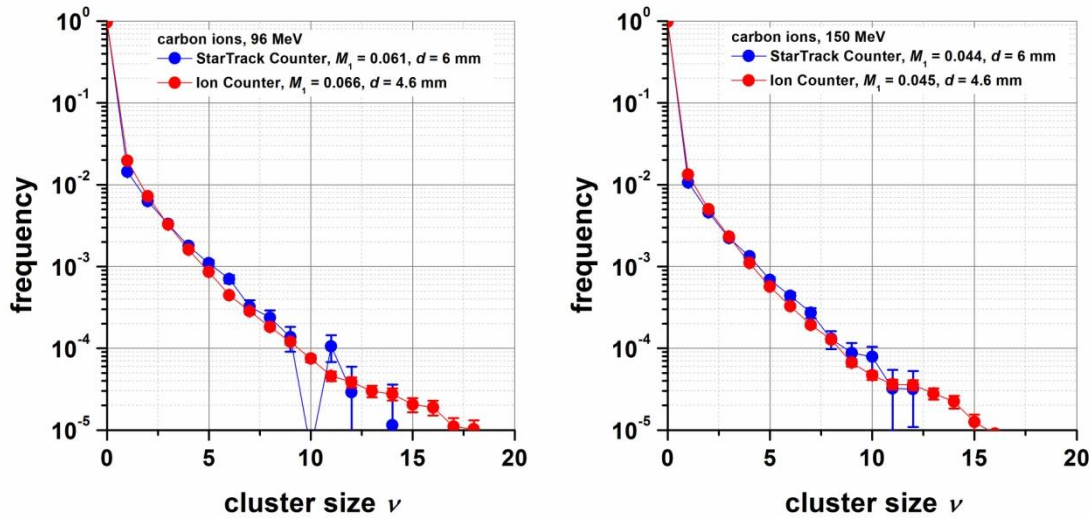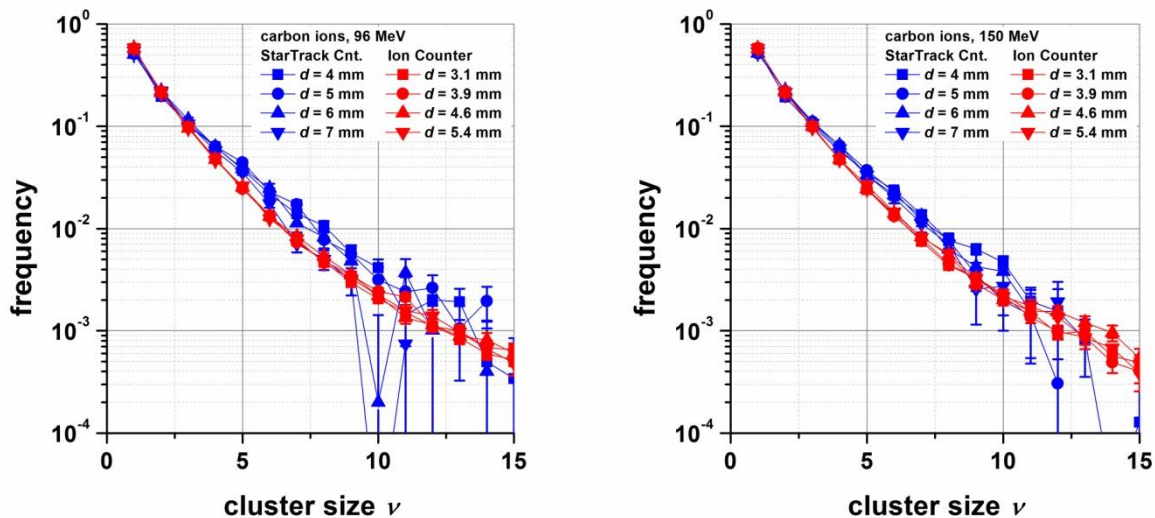
[2] V. Conte et al., New J. Phys. 14, 093010 (2012)

Figure 2.6: *Cluster size distributions measured with the StarTrack Counter and the Ion Counter in the penumbra for 96 MeV (left) and 150 MeV carbon ions for impact parameters yielding the same mean cluster size.*

Figure 2.6 shows the direct comparison of cluster size distributions measured with the StarTrack Counter and the Ion Counter in the penumbra for 96 MeV (left) and 150 MeV carbon ions. The impact parameter was d = 6 mm in the case of the StarTrack Counter and d = 4.5 mm for the Ion Counter. The impact parameters were chosen such, that the mean ionization cluster sizes M_1 were almost identical for the cluster size distributions under comparison. It is clearly visible, that the distributions measured by the two different devices are almost identical.

The similarity in shape of the distributions in the penumbra region becomes even more evident in Figure 2.7. Here the conditional cluster size distributions, i.e. the cluster size distributions for cluster size $v > 0$, are plotted for several impact parameters in the penumbra region for 96 MeV (left) and 150 MeV (right) carbon ions. The conditional distributions are almost independent from the impact parameter, and also from the particle velocity, as can be concluded from comparing the distributions for the different energies. These invariances were already observed previously[1,2]. In addition, the distributions measured with the Ion Counter are almost identical to those measured with the StarTrack Counter.
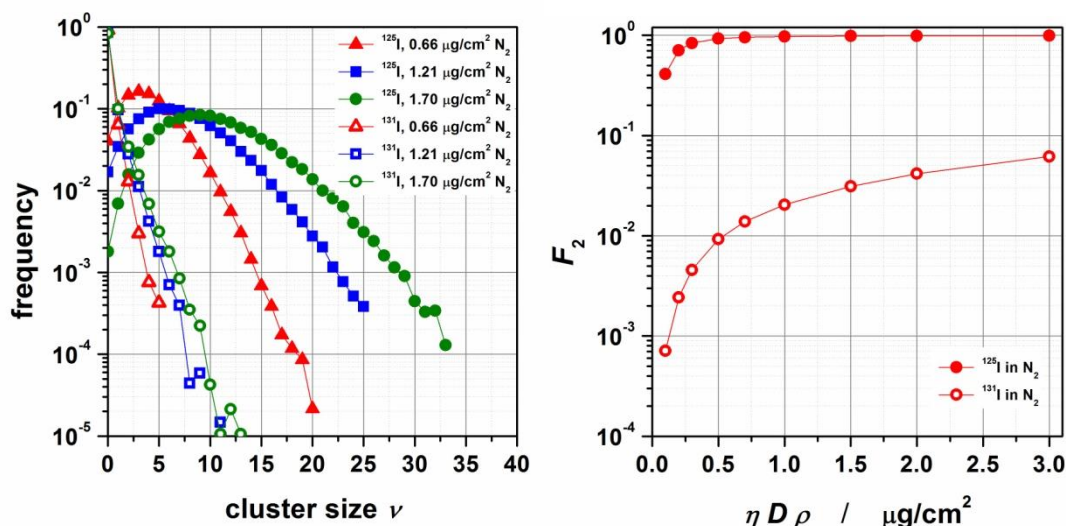

Figure 2.7: *Conditional cluster size distributions measured with the StarTrack Counter and the Ion Counter for several impact parameters in the penumbra region for 96 MeV (left) and 150 MeV (right) carbon ions.*

In total, the comparison showed that both devices, the INFN StarTrack Detector and the PTB Ion Counter, measure equivalent ionization cluster size distributions for carbon ions for passages at distances d from the target volume.

Nanodosimetry of Auger electrons (NCBJ Jet Counter)

Auger electron emitters are among the most promising radio nuclides for targeted radiotherapy, which is a method that is currently expected to be efficient in cancer treatment. The reason for this is based on the finding that Auger electron emitters release numerous short range electrons that severely damage nearby radiation-sensitive cell nucleus structures (i.e. DNA segments). For example, a source of radioactive iodine ^{125}I is an example of an Auger electron emitter that releases 13.2 electrons per disintegration[3]. The ionization cluster size distributions have been measured with the NCBJ Jet Counter for several sizes of nanometric sites when irradiated by Auger electrons from a radioactive source. The examples of such distributions are presented in Figure 2.8 (left)[4,5]. In order to compare the results for Auger electrons, the cluster size distributions from high energy electrons emitted by ^{131}I are included to show the quantitative and qualitative differences of these emitters for radiation damages of DNA.

Figure 2.8: *Ionization cluster size distributions (left) and F_2 (right) measured with ^{125}I and ^{131}I in N_2 for different target sizes $\eta D \rho$ denotes the detection efficiency for a single ion.*

The cumulative distribution probability F_2 of creating an ionization cluster of size $\nu \geq 2$ for these radioactive sources is presented in Figure 2.8 (right). As can be seen from the figures, using an Auger emitting radio nuclide like ^{125}I is much more effective for radiation treatment at DNA level than ^{131}I.

A new qualifier for radiation quality: $F_k(M_1)$ (REG(INFN) StarTrack Counter, NCBJ Jet Counter and PTB Ion Counter)

The three devices involved in the intercomparison differ in several aspects: (i) with respect to the type of secondary particles detected (electrons (REG(INFN) StarTrack Counter) or ions (NCBJ Jet Counter, PTB Ion Counter)), (ii) with respect to the target preparation (pulsed gas jet (NCBJ Jet Counter) or constant gas pressure (REG(INFN) StarTrack Counter, PTB Ion Counter)), (iii) with respect to the target gas (N_2 (NCBJ Jet Counter, PTB Ion Counter) or C_3H_8 (REG(INFN) StarTrack Counter, PTB Ion Counter)), (iv) with respect to the size of the target volume and (v) with respect to the detection efficiencies of the secondary particles.

However, the intercomparison leads to a real novelty in our knowledge of radiation interaction in nanometric

[3] E. Pomplun et al., Am. Ass. Phys. Med. Sym. Series 8, pp.137-152 (1992)

[4] S. Pszona et al., Rad. Meas. 47, 1092-1096 (2012)

[5] A. Bantsar, S. Pszona, Rad. Prot. Dos. 166, 210-213, doi:10.1093/rpd/ncv301

volumes. It is found, that, in spite of the differences among the three nanodosimeters, the data obtained with the three nanodosimeters are located on the same curve, when plotting the cumulative sum F_k of the cluster size distributions for cluster sizes $\nu \geq k$, i.e. the cumulative probability of creating an ionization cluster of size $\nu \geq k$, as a function of the mean ionization cluster size M_1. The importance of this finding is twofold: on the one hand it proves the consistency among the measurements obtained with the three nanodosimeters involved, and on the other hand it gives evidence to the existence of a family of functions $F_k (M_1)$, that is invariant with respect to both, the radiation quality of the primary ion (mass, charge and velocity) and the target properties (gas type, pressure and size), but only depends on the mean ionization cluster size M_1. Therefore this family of functions $F_k (M_1)$ together with M_1 might serve as a qualifier to describe the "nanodosimetric" radiation quality of a radiation field.

As an example Figure 2.9 shows F_2 plotted versus M_1, which is the cumulative probability of creating more than two ionization events versus the mean number of ionizations created in the sensitive volume. As can be seen clearly, the experimental values obtained with the three different devices coincide on one unique monotonic curve.
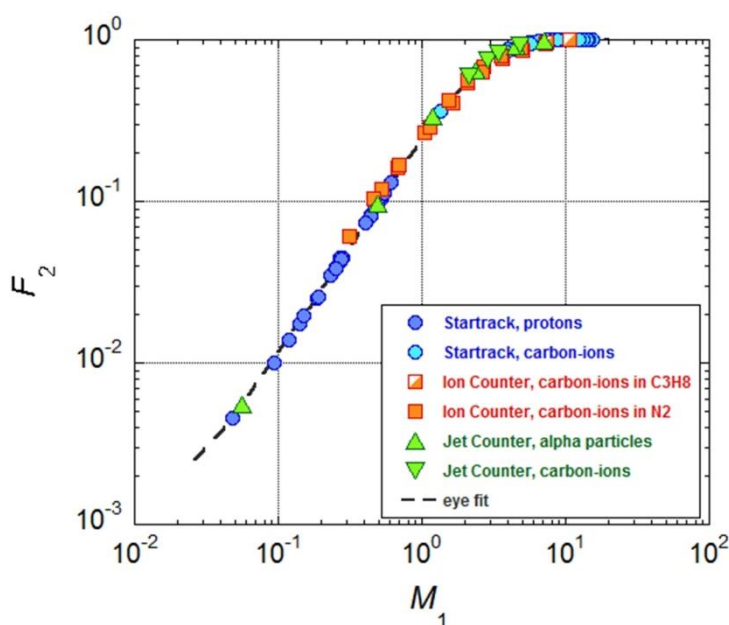
Figure 2.9: *F_2 plotted versus M_1, obtained with the three nanodosimeters for different radiation qualities and different target gases.*

Objective 3: To develop methods for measuring the production rate and 3D distribution of reactive oxygen species in tissue exposed to proton and ion beams as a function of particle type and energy.

This objective was approached by work carried out at NPL to select and then evaluate chemical "probes", each probe being chosen for its specific reactivity with one of the known products of water (tissue) radiolysis that has biological significance. Another important property of the probe was its ability to be analysed using fluorescence spectrometry techniques. Experiments were then carried out to find suitable solid matrices in which the probes could be embedded in order to carry out high resolution fluorescence microscopy on the samples and hence determine the spatial distribution of radiation induced species. A subset of this project was a small investigation carried out by NPL and the University of Palermo into the possibility of using changes in the fine structure of the EPR spectra of radiation induced radicals to provide information on the energy deposition characteristics.

Identification of selective scavengers

The first stage of the project was a literature search carried out by NPL which was based on many decades of publications on the radiolysis of water, including studies of radiation chemical yields, free radical scavengers and LET effects. This literature search was compiled using the open source JabRef system and made available to all participants in the BioQuaRT consortium.

Table 3.1 summarises the results of the literature search in terms of the selection of potential fluorescent probes, with selective reactivity towards a number of biologically important radiolytic species (OH and O_2^- radicals and molecular hydrogen peroxide).

Table 3.1: *Results of a literature search on potential fluorescent probes for different biologically relevant radiolytic species.*

Probe	ROS Detected	Excitation / Emission wavelength [nm]	Fluorescence product	Specificity	Notes
Hydroethidine (HE)	O_2^-	520 / 610	Ethidium (E)	Oxidized by a variety of ROS Reduced by cythochrome c	Interference from fluorescence from other catalysis products.
2-chloro-1,3-dibenzothiazolinecyclohexene (DBZTC)	O_2^-	485 / 559	DBZTC-oxide (DBO)	500:1 O_2^-:H_2O_2 reactivity	Long reaction kinetics (10 min?) Narrow pH range (7.2-8.2) Could be used in combination with DCFs probes (H_2O_2)
Dichlorodyhydrofluorescein (DCFH)	H_2O_2	498 / 522	2, 7-dichlorofluorescein (DCF)	Can be oxidized by other peroxides Relative insensitive to O_2^- Low reactivity with OH	2-electron process Require catalyst (Metal/HRP) HRP alone can oxidize DCFH Photo-reduction in visible and UVA
Amplex Red (AR)	H_2O_2	563 / 587	Resorufin	It requires HRP Can also be used for O_2^- with superoxide dismutase (SOD) which converts O_2^- into H_2O_2 Interference from substances that can oxide HRP	Low background High fluorescence power Further oxidation of resorufin (at very high H_2O_2 concentrations) might cause decrease sensitivity Very pH sensitive. Not stable at pH>8.3
Coumarin-3-carboxylic acid (3-CCA)	OH	350, 395 / 450	7-OHCCA	Very specific for OH	Highly sensitive to pH Well characterized (Dose, LET, pH, time, ….) Dose rate effect with no pure compound

From this list of compounds, coumarin-3-carboxylic acid (3-CCA) and hydroethidene were chosen for further study. Techniques were established for the preparation of bulk aqueous solutions of these compounds and studies were made of the radiation induced fluorescence, using a conventional laboratory spectrofluorimeter. These studies enabled characterisation in terms of the optimum excitation and fluorescence wavelengths and properties such as dose response, reproducibility, stability before and after irradiation etc.

An important aspect of objective 3 was to gain information on the LET dependence of the yields of specific biologically important radiolytic species. For example, it well known that, in general terms, the yield of radical species such as H atoms and OH radicals decreases as LET increases, whereas the yield of species such as H_2O_2, HO_2 and O_2^- increases as LET increases. As 3-CCA reacts specifically with OH radicals and hydroethidene reacts specifically with O_2^-, the ratio of fluoresce from bulk solutions of these two compounds would be expected to vary with LET. An experiment to test this was carried out using ^{60}Co radiation and 50 kVp x-rays. The results showed an indication of the expected difference in relative response, but also highlighted the problem with signal-to-noise resulting from the small fluorescence signal from hydroethidene. Because of this, experiments described below to incorporate fluorescent probes into rigid matrices were limited to 3-CCA.

Incorporation of probes into matrices

Two types of matrices were selected at NPL for experiments with fluorescent 3-CCA probes for high resolution microscopy. One was incorporation into a rigid polymer and the other a hydrogel system, such as gelatin. PMMA was selected as a suitable optically clear polymer and a series of experiments performed using different concentrations of 3-CCA. The technique used involved dissolving both PMMA and 3-CCA in chloroform, pouring the resultant thick liquid onto a glass plate and allowing the chloroform to evaporate, leaving a film of PMMA containing 3-CCA. The technique of film production was successful, but no radiation induced fluorescence could be observed in the resultant film. The reasons for this are speculative, but must include the low level of OH radical formation in the polymer, that contains only a few percent by weight of water.

It was hoped that the alternative approach of using a gelatin hydrogel would solve the problem of the lack of water to produce OH radicals, but again, no radiation induced fluorescence could be observed. The reasons in this case are more complex, as 3-CCA appeared to react with gelatin to form a fluorescent compound in the expected wavelength region in unirradiated samples, but no additional fluorescence was seen on irradiation.

The indications from this study by NPL are that 3-CCA seems to react with organic compounds (PMMA or gelatin) to produce a fluorescent compound that masks any radiation induced effect. In addition, many organic compounds are likely to be strong OH radical scavengers, which will compete with 3-CCA for OH radicals. The matrix also needs to contain a high proportion of water if any imaging results of radical distributions are to be representative of the distributions in water. Inorganic hydrogels may be one possibility to meet these requirements. Frozen aqueous solutions are another possibility, although with obvious drawbacks in terms of operating microscopy equipment at low temperatures.

Imaging methods

In parallel to the development of matrices containing fluorescent radiation induced species, work has been carried out at NPL to modify existing methods of fluorescence microscopy to enable a 3D distribution of fluorescent molecules to be produced.

Figure 3.1 shows two possible approaches: In the left hand figure, it is envisaged that the fluorescence will be imaged by repeated scans performed at different focal planes along the direction of particle tracks. A 3D distribution can then be produced by combining images from different focal planes. In the right hand figure, the irradiation is carried out in such a way that the particle tracks are at a low angle grazing incidence to the sample, allowing all fluorescent events along individual tracks to be imaged in one focal plane. Both of these methods would be compatible with existing high resolution fluorescent microscopy equipment.
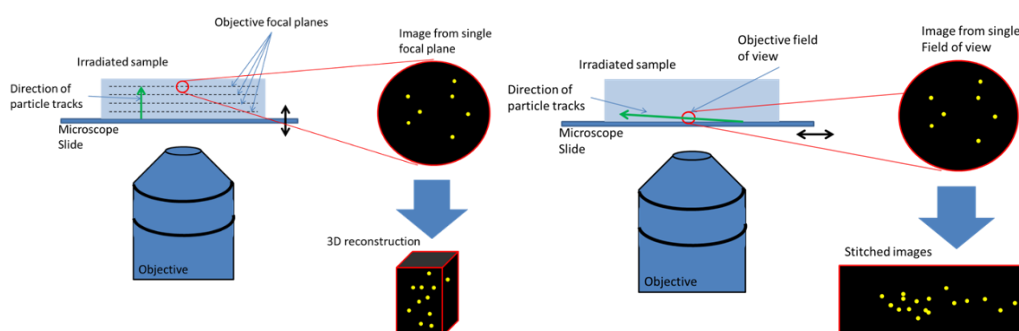
Figure 3.1: *New fluorescence 3-D microscopy methods. Left: combination of repeated scans at different focal planes along the track direction. Right: due to small incident angles between track direction and sample, all fluorescent events can be seen in the same focal plane.*

In addition to these investigations into imaging techniques, PTB investigated the possibility of performing irradiation experiments on samples containing colourimetric probes in matrices at the PTB ion microbeam. Monte Carlo simulations of the expected energy distribution within the ion tracks in such measurements

(which were eventually not carried out) were carried out by IST using the MCNP6 code and by NPL using the Geant4 toolkit.

Electron paramagnetic resonance (EPR) studies of radiation induced radicals

Differences in energy deposition due to differences in LET will influence the pattern of radiation damage in a solid crystalline structure, which will, in turn, affect the environment around radiation induced radicals. Such differences in environment may be reflected in the fine structure of the EPR spectra of radiation induced radicals. To investigate this, a detailed analysis was carried out of the EPR spectra of the radiation induced radical in the amino acid alanine. Such radicals are stable in the alanine crystal and quantitative EPR measurements in alanine are widely used as a dosimetry technique. The figure below shows high resolution spectra taken from pellets irradiated at various positions along the depth dose curve of a 60 MeV proton beam. The spectra of pellets 11, 12 and 13, in the high LET Bragg peak region are clearly different to those in the low LET region up to position 10. This experiment demonstrates the potential of EPR measurements to give information about the LET of the radiation, in addition to the absorbed dose. Aforementioned investigations were carried out by NPL.
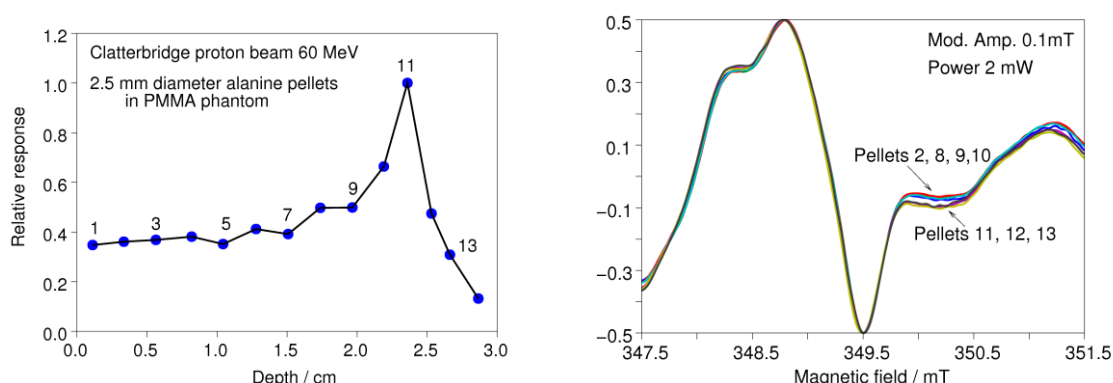
Figure 3.2: EPR response for irradiated alanine pellets at different positions along the depth dose curve of 60 MeV proton beam (Right). The response related to radical concentrations is representative of the LET of the beam for different depths (Left).

Objective 4: To develop a numerical tool (based on DNA ionization and fragmentation cross sections) for the multi-scale simulation of ionizing particle track structure and biological effects of ionizing radiation.

This objective encompassed two major research pathways:

The first was the determination of new experimental cross-section data sets for DNA constituents with the aim of augmenting track structure simulations of electrons and protons in a DNA medium and enabling the evaluation of DNA fragmentation, which indicates the probability of DNA damage by ionizing radiation. This activity was carried out at PTB for the determination of the cross-sections sets and IRSN could validate the use of the obtained data in an independent track structure code (Geant4-DNA) than the one originally used at PTB (PTB track structure simulation tool (PTra)).

The other path was dealing with the development of the multi-scale simulation tool (MST) that is based on a particular application of the Geant4-DNA Monte Carlo code. In this case, the activity was centred at IRSN but the benchmarking calculations with the PTra code at PTB or with the Particle Tracks (Partrac) code were fundamental for testing the new capabilities of the simulation tool. Theoretical guidelines concerning the

simulation of the chemical stage were given by researchers from NPL and collaborators (M. Davídková and W. Friedland).

This objective has been achieved and a new MST has been delivered. The new tool offers the capability to perform simulations at different scales (macro, micro and nanometric) combining different processes available in the Geant4 Monte Carlo code. The main developments concern the nanometric scale that now takes into account the physical, physico-chemical and chemical stages in a detailed DNA chromatine fibre and using not only liquid water cross-sections but also experimental-based DNA cross-sections and fragmentation cross sections (beyond the current state of the art of other track structure codes for radiobiology). It is thus possible to calculate simple and double strand breaks and to study their complexity in order to reproduce biological experimental data. On the other hand, the MST also allows the study of the correlation between the microdosimetric spectra obtained at the cell nucleus scale in coincidence with different radiation patterns at nanometric scale. The MST is then suitable for evaluating the different terms in a formulation proposed by the consortium for correlating the energy deposition at different scales and the biological response.

A summary of the specific work and results obtained in these activities is given below.

Cross-section data sets for DNA constituents

Low energy electron cross-section data set for DNA constituents

Total electron scattering cross-sections (TCS) of pyrimidine were measured at PTB in a linear-transmission experimental setup for electron energies between 5 eV and 1 keV. For purine, the measurements of the TCS in the current experimental setup proved infeasible owing to the low vapour pressure. The TCS of purine were calculated using the spherical complex optical potential model. A test of this model has been carried out using the experimental data of pyrimidine and showed good agreement and, hence, the applicability of this method. The data sets for pyrimidine and purine were provided.

Data sets with differential cross sections of pyrimidine and purine and electron energies up to 1 keV were provided for a) single differential elastic scattering cross sections for scattering angles between 15° and 135° and b) double differential inelastic cross-sections (in energy and angle) for the same range of emission angles and for ejection energies between 2.7 eV and the initial electron energy (up to 1 keV). The TCS of pyrimidine were measured in a crossed-beam experimental setup, while those of purine were calculated by the spherical complex optical potential model, previously tested to yield good agreement with the pyrimidine data.

Both data sets were extrapolated to the full range of scattering angles between 0° and 180° by the use of model functions from the literature. Numerical integration of the differential cross-section data was performed to obtain the additional cross-section data required for the simulation, i.e. the single differential cross-sections (as a function of secondary electron energy) as well as total ionization and total elastic scattering cross-sections. The ionization cross-section data are in accordance with the Binary-Encounter-Bethe model, which has only one free parameter and requires orbital energies of electrons in the target molecule as input data. These energies were obtained by performing a dedicated quantum chemistry model calculation. The difference between the total scattering and the ionization cross-section reproduces the total elastic scattering cross-section rather well and demonstrates the consistency of the cross section data.

In addition to the total and differential cross section data sets of the DNA nucleobase-equivalent molecules pyrimidine and purine, similar data were obtained for DNA backbone constituents tetrahydrofuran and trimethylphosphate. The data sets of electron-impact cross section data of DNA constituents were evaluated and model functions were obtained to enable a convenient implementation in simulation codes. The evaluation process, which was carried out jointly by IRSN and PTB, involved data fitting, extrapolation and integration procedures, as already described above. The parameterised model functions for each type of interaction cross section were carefully tested to satisfy consistency requirements.
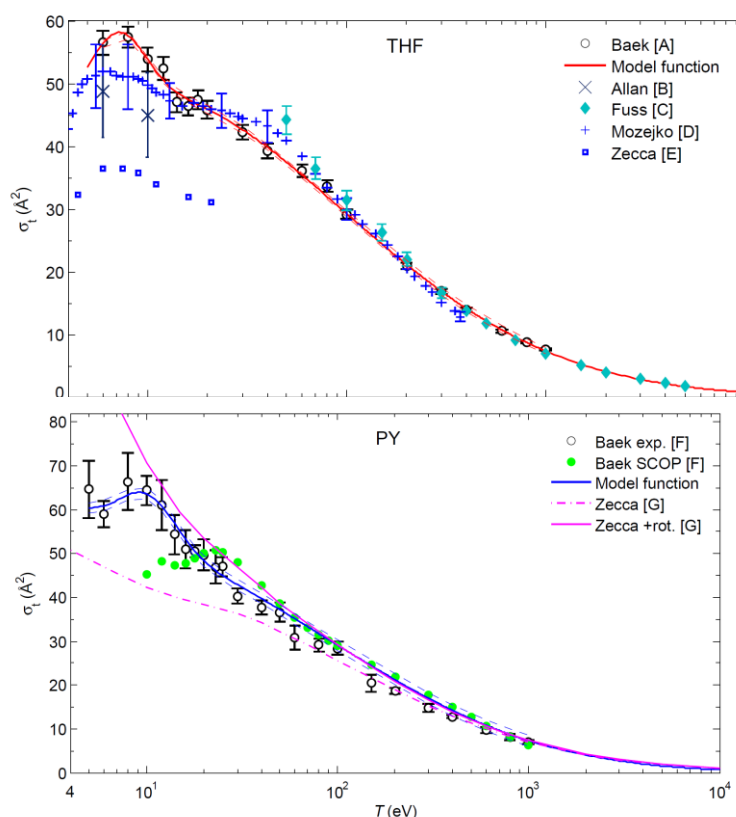
Figure 4.1: *Measured data and interpolation models for TCS σ_t of tetrahydrofuran (THF) and pyrimidine (PY) as a function of electron energy T, including experimental data of several groups (symbols). Thin lines indicate the uncertainties of the model functions.*

Cross-sections for fragmentation of DNA constituents by electrons

Relative fragmentation cross sections provide important information on the type of DNA damage. In the simulation, these data can be used after an ionization event to evaluate the breakage of specific chemical bonds.

The relative electron-impact fragmentation cross sections of the DNA constituents tetrahydrofuran and pyrimidine were measured by PTB in the energy range between 50 eV and 500 eV. The parameterisation of the measured data was performed by fitting simple model functions for each type of positively charged fragment to its probability of occurrence as a function of electron energy. Previously to the fitting procedure, the data were extrapolated by assuming a cross section of zero at the respective appearance energies.

Ionization cross-sections of DNA constituents by light ions

Double-differential ionization cross sections (with respect to the ejected electron energy and emission angle) were measured at PTB for the impact of protons with energies between 70 keV and 3 MeV in a crossed-beam arrangement for DNA-equivalent target gases tetrahydrofuran, pyrimidine and trimethylphosphate. These data are necessary for a simulation of proton tracks in a DNA medium. The aim of this work was to evaluate the measured data in order to obtain model functions, which can easily be implemented in a track structure simulation code. A requirement to the model functions is the interpolation and extrapolation of the measured double-differential cross section (DDCS) to forward and backward scattering angles. From these model functions, single-differential ionization cross sections and total ionization cross sections could be obtained.
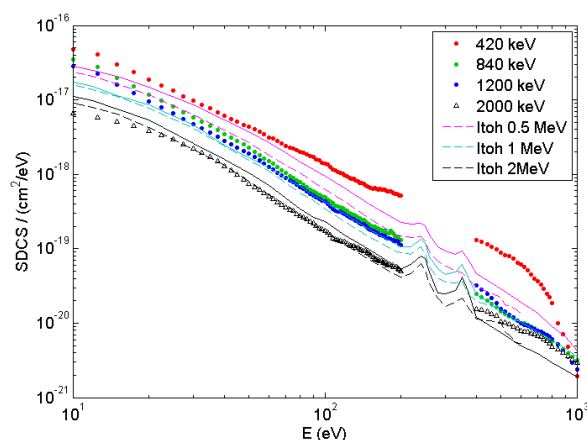
Figure 4.2. *Single-differential cross section (SDCS) of THF for proton impact ionization compared to data of Itoh et al. for uracil[6] (dashed lines) and Iriki et al. for adenine[7,8] (solid lines), which were multiplied by the ratio of valence electrons.*

Fragmentation cross-sections of DNA constituents for protons and helium ions

The setup used for the determination of cross-sections for fragmentation by electrons (D5.1.4) was adapted for experiments at the PTB ion beam facility. Fragmentation cross-sections of three chemical analogues of DNA constituents were measured. Tetrahydrofuran and pyrimidine were introduced through a supersonic jet providing high target density in a millimetre-wide interaction zone. Helium was used as the carrier gas. Due to physical damage caused by an accidental power loss, the supersonic jet was not operational in the second week so that trimethyl phosphate had to be introduced through a leak valve to flood the entire chamber with target gas. As a result, the ion spectra show wider peaks and reference spectra with the electron gun could not been taken.

The ion energies were chosen according to the microbeam energies of WP4 to compare fragmentation cross-sections to the observed damage in cells. Spectra were taken at additional energies to investigate, whether there is a difference between proton and helium ions impacting with the same velocity, and to cover a wider energy range for parameterisation.

The parameterisation of these cross section data was performed with the aim to provide probabilities for DNA damage formation following an ionization process in the track structure simulation. The following approach was elaborated: DNA damage in the form of a strand break or sugar damage results if the ring structure of tetrahydrofuran has dissociated; strand breaks result also from breakage of the P-O or O-C bonds of trimethylphosphate; finally, base damage occurs if the molecular ring structure of pyrimidine dissociates. The respective probabilities for a dissociation of the three different molecules were obtained in a two-step approach: first, the ionized molecular orbital was used to determine if the ionized mother molecule or a fragment ion was produced. In case of a fragment production, the dissociation probabilities were derived on the basis of the measured fragmentation cross sections.

Development of the multi-scale simulation tool (MST)

The MST was developed throughout the three year project. It is based on a specific application of the Geant4 Monte Carlo code[9], and, in particular, on the use of the Geant4-DNA[10] processes and models that are well suited to perform track structure calculations with nanometric detail. One of the major improvements

---

[6] A. Itoh, Y. Iriki, M. Imai, C. Champion, and R. D. Rivarola, Phys. Rev. A 88, 052711 (2013)

[7] Y. Iriki, Y. Kikuchi, M. Imai, and A. Itoh, Phys. Rev. A 84, 032704 (2011)

[8] Y. Iriki, Y. Kikuchi, M. Imai, and A. Itoh, Phys. Rev. A 84, 052719 (2011)

[9] Agostinelli, S. et al. "Geant4 – a simulation toolkit "; Nucl. Instr. And Meth. In Phys. Res. A 506, 250-303 (2003)

[10] S. Incerti et al. "The Geant4-DNA project" Int. J; Model Simul. Sci. Comput. 1, 157-178 (2010)

in the capabilities of the simulation has been to introduce the new experimental-based DNA cross-sections obtained at PTB. The implementation of these new cross-sections, their benchmark with the PTra code, and their use to evaluate double strand breaks (DSB) with probabilistic models[11], was done in parallel with the development of other capabilities of the MST, to the experimental data obtained in the radiobiological experiments.

Simulation study of microdosimetric and nanodosimetric results on cell nuclei and possible correlations

The methodology to study microdosimetric and nanodosimetric characteristics of the energy deposition within a cell nucleus was developed by IRSN at the beginning of the project using the public version of Geant4-DNA in liquid water. Two different geometries were used in the study: a homogenous ellipsoid with semi-axis a = 9.5 µm, b = 1.0 µm, and c = 5.5 µm representing the endothelium cell nucleus used in the cell irradiation experiments and a geometrical representation of the DNA molecule contained within the cell nucleus (Figure 4.3) already available[12]. For microdosimetry assessment, lineal energy and specific energy distributions were calculated in the cell nucleus for protons, alpha particles and carbon ions covering a wide range of LET. The same projectiles were used to characterise the energy deposition in the DNA molecule that can be at the origin of direct effects. To do so, only energy depositions (either by ionization or excitation processes) that were located on the back-bone region of the DNA geometry were considered as possibly being responsible for direct breaks. After the selection of these energy transfer points, a clustering algorithm (density based scan (DBSCAN[13,14])) was used in order to search for those that were close enough to correspond to double strand breaks (DSB).
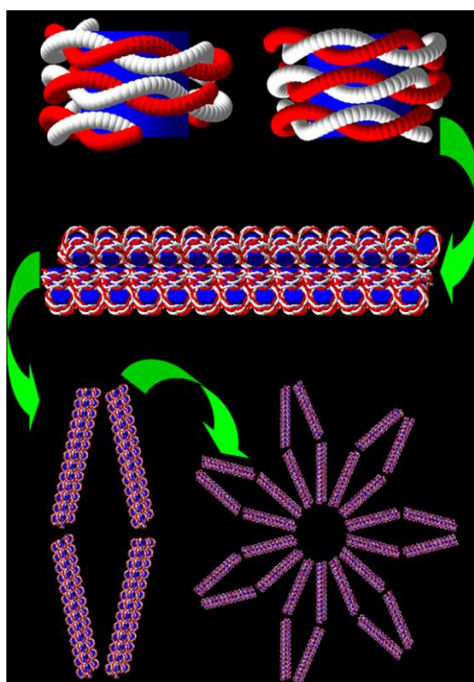
Figure 4.3. *First geometry of the DNA chromatin[12] used in this project for the target description within the MST. In this geometry, 5 levels of the DNA are represented: Double helix (separating back-bone region and bases), nucleosomes, 30 nm diameter chromatin fibres, simple loops and complex loops (rosette). Using the loop compaction, the whole cell nucleus was filled up to completing the 6 Gbp in a eukaryotic cell.*

---

[11] G. Garty, R. Schulte, et al. Radiat Prot Dosim 122, 451–454 (2006)

[12] M. Dos Santos, C. Villagrasa, I. Clairand and S. Incerti. "Influence of the DNA density on the number of clustered damages created by protons of different energies". Nucl. Instrum. Meth. B 298, 47-54 (2013)

[13] Martin Ester, Hans-Peter Kriegel, Jörg Sander, Xiaowei Xu. "A density-based algorithm for discovering clusters in large spatial databases with noise", in: Evangelos Simoudis, Jiawei Han, Usama M. Fayyad (Eds.), Proceedings of the Second International Conference on Knowledge Discovery and Data Mining, AAAI Press, pp. 226–231 (1996)

[14] Z. Francis et al., "Molecular scale track structure simulations in liquid water using the Geant4-DNA Monte Carlo processes. Appl. Radiat. Isot. 69, 220-226 (2011)

This DBSCAN clustering algorithm basically requires three main parameters: the radius of the neighbourhood area, the minimum number of points needed to form a cluster and the minimum energy contained in that cluster (the energy being the amount of the energy transferred at that position). From these parameters, the result of the algorithm will reveal clusters having a maximum radius defined by the input parameter and a variable number of points within that will give us the information about their complexity. Points that would not match the input conditions will appear as isolated points. The parameters used in this work to form a cluster correspond to the classical definition of a DSB: minimum of two points separated by less than ten base pair's distance and at least one of the points in the cluster located in a different strand than the others. The energy threshold of the cluster (8 eV) was set allowing all types of energy transfer points (ionization or excitation) to be taken into account. A first attempt to study the correlation between microdosimetric and nanodosimetric results obtained by the simulation was made. Nevertheless, this correlation was focused on the mean values of the resulting distributions (and thus losing important information contained in the standard deviations) and this has taken into account the amount of energy deposited in the target, what has been revealed, at the end of this project as not being the best quantity to link both scales. Instead of the energy, the number of ionizations (or ionization clusters distribution) has appeared as being more suited to define new quantities relating the irradiation conditions and the biological response.

At the midterm of this project, a generic mathematical model for correlating energy deposited at micrometric and nanometric scales was proposed after intensive discussions among PTB, NPL, IRSN, IST and ENEA[15]. In this formula, the terms describing the energy deposition were separated from those concerning the biological response of the target. The main term describing the physical characteristics of the irradiation corresponds thus to the conditional probability that irradiation of a biological system with radiation quality Q to a macroscopic absorbed dose D will lead at the end of the physicochemical stage to a particular initial radiation damage pattern. This probability takes into account the conditional probabilities between a given ionization cluster size distribution at nanometric scale and a given lineal energy distribution at micrometric scale leading to the radiation damage pattern studied. All these probabilities have the advantage of being measurable. The main unknown parameter remaining is the definition of the sensitive volume in which performing the measurements will allow a simple formulation of the correlation.

Benchmarking with other Monte Carlo codes

Several benchmarks of the track structure simulation achieved with the public version of Geant4-DNA using the liquid water cross-sections have been made during the development of the MST. These benchmarks were performed in joint work by IRSN, IST and PTB in order to better characterise the nanodosimetric and microdosimetric results obtained with respect to well-known codes in both scales: nanometric (PARTRAC or PTra) and micrometric (MCNPX and MCNP6. In the nanometric scale, it was shown that, in general, the cross-sections used in Geant4-DNA for electrons of low kinetic energy < 100 eV are larger than those used in PTra or PARTRAC. For ion projectiles, the consequences are visible in terms of the ionization cluster size distribution obtained when the target volume is large enough to contain an important contribution of the secondary electrons (ex: nucleosome dimensions). Concerning the micodosimetric spectra obtained within the whole cell nucleus, the comparison of results found between Geant4-DNA and MCNPX or MCNP6 showed quite good agreement. No differences were found between the results of both of these codes (MCNPX and MCNP6) at this scale.

Augmented version of the track structure code with the DNA cross-sections

As explained before, the new cross-sections for DNA materials obtained by PTB (for both protons and low energy electrons) were implemented in the MST (IRSN's "home" version of Geant4-DNA). The implementation was not straightforward as the Geant4-DNA class design is used for only one material (liquid water) so a new model class design had to be build.

---

[15] Palmans, H. Rabus, H. et al. "Future development of biologically relevant dosimetry", British Journal of Radiology 87: 20140392 (2015)

The implementation was validated by comparing IRSN's results using the MST with those obtained by PTB with the Monte Carlo code PTra that also included the new cross-section sets in a new augmented version. Using both augmented codes, calculations were performed based on the probabilistic model of Garty and Schulte[11] concerning the number of expected DSB using a DNA medium composition. On the other hand, both augmented codes were also used for the evaluation of ionization cluster size distributions (ICSDs) in 10 base pair cylinders at different distances of a 8 MeV proton track in order to simulate the experimental procedure used in nanodosimetry (objective 2). As it can be seen in Figure 4.4, the mean value of the ICSDs as a function of the impact parameter corresponds to the well-known shape obtained in the experiments. The differences in the values obtained with both codes correspond to the use of different cross-section for the liquid water material that enter (together with those of the DNA constituents as measured by PTB) in the composition of the DNA medium.
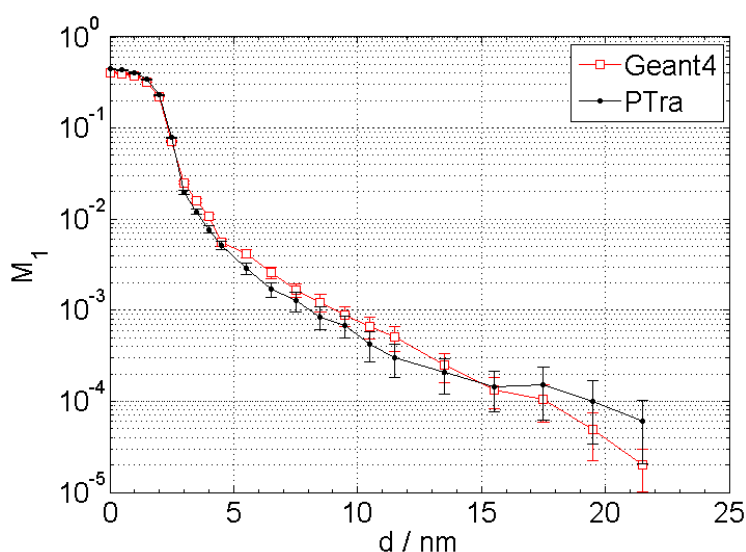
Figure 4.4. *Mean ionization cluster size M1 as a function of impact parameter d.*

Including the simulation of indirect effects

In order to be able to simulate the early biological effects, it seemed necessary to include in the simulation a description of the production of the indirect effects on the DNA molecule: breakages of the DNA molecule produced by the radio-induced radicals around the DNA (about 4-5 nm), in particular by the OH· radical.

Again, as in the simulation of the track structure and its intersection with the DNA geometry (physical stage) it was decided by IRSN and PTB to base the simulation of this new part (physico-chemical + chemical stage) on a Geant4-DNA application. Indeed, several codes dedicated to radiobiology allow the simulation of the chemical stage (as PARTRAC[16] or RAdiation DAmage to bioMOLecules (RADAMOL)[17]) and the presence of their authors as collaborators of this consortium was crucial to the extension of the MST to the simulation of indirect effects. Nevertheless, the extension of the MST in the basis of a Geant4-DNA application (instead of using other existing code) presents several benefits as the use of the same DNA geometry for the assessment of both direct and indirect effects and the possibility of implementing different parameters than the ones of other codes concerning for example, the scavenging reactants or the time steps considered in the simulation.

The public version of the Geant4-DNA models (v 10.01) included the classes needed to perform the simulation of the physico-chemical stage (creation of radicals after the energy deposition of the ion track) and

---

[16] Friedland W, Dingfelder M, Kundrát P, Jacob P. Track structures, DNA targets and radiation effects in the biophysical Monte Carlo simulation code PARTRAC. Mutat. Res. 711, 28-40 (2011)

[17] V. Stepan and M. Davidkova."RADAMOL tool: Role of radiation quality and charge transfer in damage distribution along the DNA oligomer". Eur. Phys. J.D. 68: 240 (2014)

the chemical stage (main reactions concerning the water radicals and the solvated electrons)[18]. The main objective in this work was to include in the simulation the interaction between the water radicals and the DNA molecules, differentiating reactions with the deoxyribose (that can lead to a break of the helix) and with the bases.

To do so, a new description of the DNA molecule was introduced by IRSN in the calculations (for both the physical stage and the chemical stage) replacing the one in Figure 4.3. Indeed, the previous geometry presented realistic volumes for the different DNA parts but it did not individually determine the position of each sugar, phosphate or base. A new geometry based on Protein Data Bank (PDB)[19] files was thus introduced with the required molecular detail. Nevertheless, because the long computing time in the simulations including the chemical stage, the DNA geometrical target was limited to the 30 diameter chromatin fibre (see Figure 4.5).

The position of the DNA constituents was taken into account in the simulation of the chemical stage by including them in the table of radicals transported, but with a diffusion coefficient equal to zero (their position was thus preserved) (see Table 4.1). They were also implemented in the table of possible chemical reactions using the reaction rates constants given by Aydogan et al.[20,21]. Only the reactions between the OH radical and the deoxyribose or the bases were taken into account. On the other hand, the histone proteins were represented in the simulation as scavengers because, every radical or solvated electron entering in contact with the histone proteins was deleted from the rest of the simulation.

In order to evaluate the number of simple (SSB) and double strand breaks obtained for different ion projectiles using the MST, the following considerations were used by IRSN and PTB: during the simulation of the physical stage, each ionization located on a sugar or phosphate volume is at the origin of a direct SSB. Concerning the chemical stage, the chemical reaction between an OH radical and a deoxyribose will lead to an indirect SSB in only 40 % of the cases[17]. Finally, the DBSCAN algorithm is used on the resulting SSB either by direct or indirect effects using the proximity criteria (and their strand label) in order to calculate the number of DSB. The use of the clustering algorithm also gave us the possibility to extend the research to other definitions of damages such as the complex DSB using other proximity criteria.
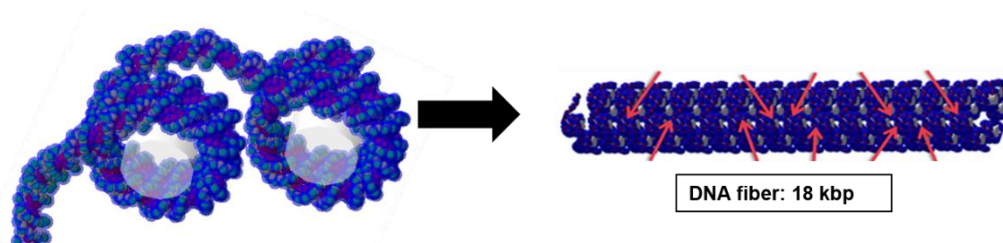
Figure 4.5. *New geometry used for the simulations of the physical stage followed by the physico-chemical and the chemical stages in this work. Different molecular components of DNA are individually identified (sugar, phosphate, bases, histones) and represented as cut spheres (avoiding overlaps for the simulation) with realistic volumes. The double helix and the chromatin fibre compaction levels of the chromatin are taken into account.*

---

[18] M. Karamitros, S. Luan, M.A. Bernal, J. Allison, G. Baldacchino, M. Davidkova, Z. Francis, W. Friedland, V. Ivantchenko, A. Ivantchenko, A. Mantero, P. Nieminem, G. Santin, H.N. Tran, V. Stepan, S. Incerti, J. Comput. Phys. 274, 841-882 (2014)

[19] Online at: http://www.rcsb.org/pdb/static.do?p=file_formats/pdb/index.html

[20] B. Aydogan, D.T. Marshall, S.G. Swarts, J.E. Turner, A.J. Boone, N. G. Richards and W.E.Bolch. "Site-specific OH attack to the sugar Moiety of DNA: A comparison of experimental data and Computational Simulation" Rad. Res. 157, 38-44 (2002)

[21] B. Aydogan, W.E. Bolch, S.G. Swarts, J.E. Turner and D.T. Marshall "Monte Carlo simulations of site-specific radical attack to DNA bases". Rad. Res. 169, 223-231 (2008)

Table 4.1: *Chemical diffusion coefficients and reactions rates used in the simulation of the chemical stage.*

Chemical species	Diffusion coefficient (m2/s)
H2	5×10^{-9}
H2O	2×10^{-5}
H2O2	1.4×10^{-9}
H3Op	9×10^{-9}
OH	2.8×10^{-9}
OHm	5×10^{-9}
e_{aq}	4.9×10^{-9}
H	7×10^{-9}
Desoxyribose	0
Adenine	0
Guanine	0
Thymine	0
Cytosine	0

Chemical reactions	Reaction rate (10^{-3}m3/mole*s)
$e_{aq} + e_{aq} + 2H2O \rightarrow H2 + 2OH^-$	0.5×10^{10}
$e_{aq} + OH^* \rightarrow OH^-$	2.95×10^{10}
$e_{aq} + H^* + H2O \rightarrow H2 + OH^-$	2.65×10^{10}
$e_{aq} + H3O^+ \rightarrow H^+ + H2O$	2.11×10^{10}
$e_{aq} + H2O2 \rightarrow OH^- + OH^*$	1.41×10^{10}
$OH^* + OH^* \rightarrow H2O2$	0.44×10^{10}
$OH^* + H^* \rightarrow H2O$	1.44×10^{10}
$H^* + H^* \rightarrow H2$	1.20×10^{10}
$H3O^+ + OH^- \rightarrow 2H2O$	14.3×10^{10}
$^1Desoxyribose + OH^*$	2.5×10^9
$^1Adenine + OH^*$	6.10×10^9
$^1Guanine + OH^*$	9.20×10^9
$^1Thymine + OH^*$	6.40×10^9
$^1Cytosine + OH^*$	6.10×10^9

Objective 5: To develop quantitative models to link the physical quantities with the biological outcome and to determine free parameters in the multi-scale model from biological assays.

The experimental data on early effects (γ–H2AX and 53BP1 foci) were measured after microbeam irradiation of endothelium cell nuclei by IRSN. Late effects on chromosomal aberrations, di-centrics and micronuclei were also measured at the PTB microbeam for the same projectiles (protons and alpha particles for different LETs) by ENEA and IST. One of the major achievements of this work consisted of developing an experimental procedure using microbeam irradiations in order to correlate the biological measurements to a specific fluence of the projectiles.

Thanks to this correlation, it was possible to compare the biological results obtained with the results of the simulation. In the case of early effects, the MST was extended in order to simulate the irradiation of cells and to calculate the number of expected foci. A direct comparison with the experimental data showed an overestimation in the simulated results. Concerning the comparison with the experimental late effects, the results of the MST on the number of complex cluster lesions were used as input parameters in the code BIophysical ANalysis of Cell death and chromosome Aberrations (BIANCA) that is able to calculate di-centrics and chromosome aberrations. This comparison confirmed the overestimation of the simulation results but indicated a good behaviour in terms of the projectile LET dependence. These results will allow us to identify the parameters in the simulation (especially in the chemical stage simulation) that can be at the origin of the overestimation and must still be fixed in the future (see below for details).

A summary of the specific work and achievements in these activities is given below:

Experimental data on early biological effects

The aim of the joint research by IRSN and PTB concerning early biological effects was to develop a procedure for the measurement of the probabilities of DNA damage induced by accelerated, focused protons and He ions. This would provide a first data set to be used as a benchmark for the predictions of the multi scale model. There were three steps to achieve this goal. The first was to develop the protocol for immunofluorescence labelling, microscopy acquisitions, and analysis of microscopy images for the detection and analysis of γ–H2AX and 53BP1 foci that are correlated to DNA damage sites. The second was to perform the microbeam irradiations and to characterise the different parameters of these irradiations that could have an impact on the foci occurrence. The last step was to format the raw data taking into account the microbeam parameters in order to compare biological results with the results obtained using the multi scale simulation tool.

Biological experimental design

The cell nuclei were irradiated with a certain pattern of ionizing particles of different nature and energy at the microbeam facility at PTB. Cultures of primary cells such as HUVEC cells (Human umbilical vein endothelial) were exposed to 8, 10 or 20 MeV α particles with respective calculated LET at the position of the cell of 160, 90 and 37 keV μm^{-1}, or to 3 MeV protons with a calculated LET of 23 keV μm^{-1}. Each cell nucleus was hit by a pattern of 5 particles placed at the extremity square of 4 μm side with one in the middle positioned at the barycentre of each cell nucleus. Ten and thirty minutes after irradiation, the cells were fixed and immuno-labelled for the detection and analysis of $\gamma-$H2AX and 53BP1 foci that are correlated to DNA damage sites. The microscopy acquisition and image analysis were performed at IRSN. Distributions of the number of foci per nucleus were obtained for each energy and particle quality studied. No significant difference was observed between the distributions observed at 10 and 30 minutes post exposure for a given LET.

Simulation of hit occurrence during microbeam irradiation

In this work, each cell nucleus of a population has been targeted with the same pattern of irradiation using the microbeam facility at PTB. However, the real size of each nucleus associated with microbeam characteristics such as beam size or detection thresholds and noise events in the particle counter could deform the square shape of the pattern and then the real number of particles reaching the nucleus. Hence to obtain a probability of foci formation per track, an accurate estimation of the real number of particles reaching nuclei was done.

To estimate how features can affect the real number of hits and their localisation, calculations were undertaken. For each irradiated dish, each nucleus of the cell population was simulated as an ellipse considering major and minor axes, together with its orientation obtained following automated image analysis. The beam size and detection thresholds and noise events in the particle counter were also taken into account in this evaluation. For around 10 % of cell nuclei the irradiation characteristics led to less than 5 particle hits. The data concerning foci background, probabilities of foci formation due to a given particle track, and characteristics of microbeam irradiation were formatted in order to be used and compared to the results of the multi scale simulation.

Experimental data on the repair of early biological effects

As an intermediate step between the induction of DSBs as early biological radiation effects and the late effects described below, additional investigations into the repair of radiation-induced foci have been carried out. The purpose was to obtain data on the dependence of repair kinetics on radiation quality. Assisted by IRSN, ENEA and IST, REG(IST-ID) performed Irradiations of a HUVEC cell line with 3 MeV protons and 8 MeV, 10 MeV and 20 MeV alpha-particles. The radiation source was the ion microbeam operated by PTB. Applying the 53BP1 assay, the number of DSBs induced by the different radiation qualities was assessed at times of 30 minutes and 2, 4, 8 and 24 hours after the irradiation. From the data, the yield of early effects of the radiation have been obtained and the kinetics curves of the DNA-repair processes have been determined.

Experimental data on late biological effects

Radiobiology experiments concerning late effects were performed in collaboration between ENEA and IST. Within the BioQuaRT objective aimed at developing quantitative models to link the physical quantities with biological data, these experiments were performed in order to evaluate the late or 'processed' DNA damage, i.e. the permanent damage that can be observed as a consequence of the cellular machinery's attempt, and partial failure, to repair the early damage induced at the time of irradiation.

Charged-particle microbeam facilities were chosen as the platforms for radiobiology experiments, because they permit us to target single cells (or compartments of a cell) with a predefined number of ionizing particles and correlating the cell-by-cell induced damage with type and energy of the radiation and with the number of ions per cell.

In order to analyse the unrepaired chromosome damage induced by microbeam irradiations two biological endpoints were chosen: the di-centric chromosome assay and the micronucleus test. For this purpose, a

novel in situ protocol was developed on a Chinese hamster ovary (CHO) cell line for carrying out cell irradiations at the PTB ion microbeam facility. This in situ protocol allows the simultaneous scoring of chromosome aberrations and micronuclei on the same irradiated sample, optimising experimental conditions in which only a very low number of cells can be seeded for the irradiation. Moreover, the method is able to distinguish metaphases in the first cell division (M1) from those in the second cell cycle (M2) by means of the difference of chromosome number, utilising the inhibition of cytokinesis induced by cytochalasin B.

CHO cells were irradiated with different radiation qualities (the same as those used for early effects plus protons at 4.8 keV/μm): accelerated, focused, and counted protons and alpha particles, including an alpha particle radiation quality simulating ^{12}C ions (160 keV/μm). Radiation-induced chromosome damage was quantified and the frequencies and distribution of di-centrics, centric rings and excess acentric fragments and of micronuclei were obtained.

It is worth noting that the experimental data produced within BioQuaRT are the first set of data on chromosomal aberrations provided after microbeam irradiation.

As regards the irradiation with alpha particles at the same dose, 10 MeV alpha particles (LET ~ 90 keV/μm) were more effective, by a factor of about 2 or even more, also depending on the considered endpoint, than 20 MeV alpha particles (LET about 37 keV/μm), in accordance with the differences in LET at inducing severe DNA damage that can lead to chromosome aberrations.

The experimental data were compared with the outcomes of a theoretical model (BIANCA) based on DNA complex damage and chromosome fragment mis-rejoining. The comparison between simulated and observed aberrations allowed us to interpret the experimental results in terms of the radiation effectiveness at inducing DNA cluster lesions.

Linking track structure to biological response

Comparison with early damages

The simulations corresponding to early effects were performed by IRSN with consultancy from PTB using as a target the 30 nm diameter chromatin fibre presented in Figure 4.5. In order to extrapolate the results to the whole cell nucleus, a scaling procedure[22] was used. In this procedure, chromatin fibres were compacted in 1 Mbp chromosome domains that are uniformly and randomly distributed in the cell nucleus volume. Inside each chromosome domain, the chromosome fibres are also uniformly distributed. A Monte Carlo calculation was used to place the chromosome territories with a mean free path of $\lambda = 1/(N\sigma)$ = 388 nm with N being the number of chromosome territories in the cell nucleus and σ the geometrical cross-section of the spherical domain of 0.2 μm radius. In the same way, the mean free path used to place each chromatin fibres in the chromosome domain is λ_{fibre}= 179 nm. The result of this calculation is a distribution in the number of fibre that an ion track crosses through the cell nucleus in the z direction (2 μm height). The convolution of this distribution with the one on the number of DSB simulated per fibre, give us the number of DSB per track crossing the cell nucleus.

The simulation was thus performed for the four projectiles used in the microbeam experiments for early effects (and one more for the late effects), namely protons with LET in the centre of the cell nuclei of 23 keV/μm and alpha particles of 37, 90 and 160 keV/μm (plus protons of 5 keV/μm for late effects). In order to compare with the experimental histograms of 53BP-foci obtained in the respective radiobiological assays, the number of DSB simulated with the MST along the track were taken into account together with a simulation of the microbeam irradiation (position of the beam, orientation of the cell nucleus, etc.) and a projection of the resulting DSB on the image plane. Finally, the mean size of a foci (that can "hide" several projected DSB) was also taken into account. The final comparison between the simulated and the experimental histograms is given in Table 5.1 where the mean values of the histograms are presented. The table shows for all the projectiles an overestimation of the number of foci in the simulations.

This overestimation can be due to different factors. In particular, it can be caused by the choices made in the simulation of the chemical stage (diameter of the histone proteins, reaction rates, treatment of the forbidden volumes, etc.). On the other hand, the biological experimental data can also underestimate the number of

---

[22] B. Lee, PhD thesis, Georgia Institute of Technology, 2014

DSB produced as they represent a "fixed picture" of the cell signalisation of damage at a given time and it is not completely known whether this signalisation depends on the time after the irradiation or, for example, the chromatin structure at the precise position of the damages. All those possible explanation factors, from the simulation and the biological point of view, should be investigated in future work.

Table 5.1: Mean values of the experimental and simulated histograms representing the number of foci/nucleus when cells are irradiated with 5 particles per nucleus.

	Protons 23 keV/µm	**Alpha particles 37 keV/µm**	**Alpha particles 90 keV/µm**	**Alpha particles 160 keV/µm**
Experimental mean value	1.59	2.31	3.44	3.29
Simulated mean value	2.93	3.83	5.08	5.37

Extension to late effects

The extension of the MST to a comparison to late effects experimental data was made by IRSN, ENEA and PTB, NPL and IST together with collaborator UniPv, making use of the existing code BIANCA[23,24,25], a biophysical model of radiation-induced chromosome aberrations and cell death developed by collaborator University of Pavia The model, which is implemented as a Monte Carlo simulation code, is based on the hypothesis that DNA "Cluster Lesions" (CLs) induced within a threshold distance d lead to chromosome aberrations. In the current version of the model, the mean number of CLs per Gyand per cell and d are two adjustable parameters. In the first part of the work, the model was applied in its 'standard' version, finding good agreement with chromosome-aberration data obtained by ENEA/IST exposing CHO hamster cells to protons or alpha particles of different energy at the PTB microbeam facility. The comparison between simulated and observed aberrations allowed the interpretation of the experimental data in terms of the radiation effectiveness at inducing DNA cluster lesions, which was found to be both ion- and energy-dependent. The CLs values leading to good agreement with experimental data on chromosome aberrations are given in columns 7 and 8 of Table 5.2.

Table 5.2: Calculated (BIANCA) and experimental yields for di-centrics, centric rings and acentric fragments for the three considered radiation qualities.

Ion	E(MeV)	LET(keV/µm	Number of ions	DIC+CR	ACE	CL/ion	CL/cell
α	10	90	10	0.61 *(0.60)*	0.82 *(0.69)*	0.69	7.4
α	20	37	25	0.35 *(0.36)*	0.56 *(0.21)*	0.20	5.3
p	10	5	200	0.35 *(0.36)*	0.52 *(0.15)*	0.024	4.8

Subsequently, with the aim of characterising these "Cluster Lesions", they were calculated from the simulated data obtained with MST as explained above. In order to calculate the number of CLs to be used by the BIANCA code, different parameters were used to a complex DSB, as explained below:

- Type 1: At the base pair level, a complex DSB is defined as at least two DSBs within 30 base-pairs (this definition corresponds to the so-called DSB++ introduced by Goodhead and others).

[23] Ballarini F. et al. "From DNA Radiation Damage to Cell Death: Theoretical Approaches, Journal of Nucleic Acids", Vol. 2010, Article ID 350608, 8 pages, doi:10.4061/2010/350608

[24] Ballarini F., Altieri S., Bortolussi S., Giroletti E., and Protti N., "A model of radiation-induced cell killing: insights into mechanisms and applications for hadrontherapy", Radiat. Res., Vol. 180, 307-315 (2013)

[25] Ballarini F., Altieri S., Bortolussi S., Carante M., Giroletti E., and Protti N., "The BIANCA model/code of radiation-induced cell death: application to human cells exposed to different radiation types", Radiat. Environ. Biophys., Vol. 53, 525–533 (2014)

- Type 2: At the kbp level, complex DSB is defined as 2 DSBs separated by a minimum of 100 bp and a maximum of 2 kbp (this definition corresponds to DNA fragments of about 2 kbp, which are interesting because they are related to the winding of the double helix around a nucleosome and the packing of nucleosomes in the chromatin fibre). In this work, we also calculated complex DSBs type 2 with the parameters: minimum distance of 200 bp and a maximum of 4 kbp.

In order to evaluate the number of CLs per track traversing the whole cell nucleus, the "scaling" procedure explained above was used. Nevertheless, the cell nucleus description used this time corresponds to the dimensions measured in the late effects experiments: a cylindrical cell nucleus of V=165 µm^3 and height 3.34 µm. Concerning complex DSBs of type 1, the yields (mean number of complex DSBs per track) calculated were much higher than the CLs yields expected in order to obtain a good agreement with the experimental results, being 0.037, 0.764 and 3.9 for 5 keV/µm protons, 37 keV/µm alpha particles and 90 keV/µm alpha particles, respectively. As a consequence, using them as input for the BIANCA code, led to an important overestimation of the observed chromosome aberration data: even in the "best case", which was that of 5 keV/µm protons, the calculated di-centrics plus centric rings were about 0.74/cell, which is more than double the observed yield. When definition 2 was applied, the yields calculated became closer to the CL yields expected: while no event was scored for 5 keV/µm protons due to statistics-related issues, the mean number of complex DSBs of type 2 per track was 0.083 for 37 keV/µm alpha particles (to be compared with 0.20) and 1.25 for 90 keV/µm alpha particles (to be compared with 0.69). As expected, using these yields as input for BIANCA led to an underestimation of chromosome aberrations induced by 37 keV/µm alpha particles and an overestimation of those induced by 90 keV/µm alpha particles. In particular, the calculated yields of di-centrics plus centric rings for 90 keV/µm alpha particles were about 1.37, to be compared with an experimental yield of 0.60. The conclusions obtained from the extension of the simulated early damages results to late effects evaluation agree with the overestimation found before. Nevertheless, testing different assumptions on the molecular features of this cluster damage suggested that clusters of DSBs at the kilo-base-pair scale ("regional clustering"), which corresponds to the nucleosome level, might better correspond to this critical DNA damage than DSB clusters at the base-pair scale ("local clustering"). However, this needs to be further tested in the future with a more systematic approach.

Investigation of pathways to use the multi-scale model for treatment planning

As a prerequisite for future exploitation of the results obtained in this joint research project, complementary investigations were carried out into the question how track-structure derived quantities could be translated towards clinical applications in ion therapy. Based on track structure simulations performed by IRSN for protons and carbon ions in a clinically relevant energy range, REG (MRI) and PTB have derived parametric models of track structure characteristics whose adjustable parameters were obtained by fitting to the Monte Carlo simulation results. Based on these models, a prototype tool has been implemented which enables a fast calculation of macroscopically relevant mean values with the help of weighting functions for the track structure parameters. Furthermore, a validation experiment was designed in order to test this weighting approach.

Summary and conclusions

- The feasibility of direct measurement of the microdosimetric quantity lineal energy in tissue equivalent absorbers using micro-calorimeters has been demonstrated.

- The first European characterisation of a clinical carbon ion beam by microdosimetric measurement has been conducted.

- The first ever intercomparison of nanodosimeters for measuring carbon ion track structure at the nanometre level has been conducted and the scaling principle of nanodosimetry has been verified.

- The functional relations between cumulative probabilities and the mean ionization cluster size have been found to match the dependence of radiobiological effects as a function of radiation quality.

- The feasibility of measuring the spatial distribution of radical species in ion tracks has been proven in principle.

- A prototype multi-scale combined micro- and nanodosimeter has been developed and used to provide the first ever well-characterised ion beams for radiobiological assays.

- A simulation tool for the multi-scale modelling of biological effects of ion beam radiation has been developed that builds on DNA interaction cross sections and, hence, allows more realistic modelling of biological radiation effects. The newly developed simulation tool has been used with the radiobiological reference data and to establish a quantitative link between particle track structure and the biological effect of ion radiation.

- A possible path for the take-up of the multi-scale approach by radio-oncologists in treatment planning has been demonstrated.

4   Actual and potential impact

Dissemination of results

The project outputs have been shared widely with the metrology, instrumentation and clinical communities. There were 108 presentations at international scientific conferences, 42 articles published in peer reviewed journals, 16 training courses, 4 workshops, 8 reports to international standards committees, and 37 other dissemination activities such as web sites and seminar or workshop presentations. Collaborators and stakeholders were regularly updated formally and informally. Discussions were held with the International Commission for Radiological Units and Measurements about establishing a reporting committee based on the outcomes of the project. A representative of the International Atomic Energy Agency was invited to PTB for a presentation of the project results and consultation about potential uptake. A symposium was held as part of the 3rd ESTRO forum with an audience of about 200 people.

Early Impact

The project brought together the clinicians, biologist and physicists in this field and generated a collaborative approach to the problem. It demonstrated the importance of understanding both the physics and biological processes in order to characterise the ion beam radiation fully and accurately.

The project has had a significant impact on European research institutions active in the field of ionising radiation metrology. PTB has created a new department within its ionising radiation division to focus on radiation effects. The results have been shared with IAEA and ICRU, who are the standardising bodies active in this area.

The results are being used in studies in the US into the potential benefits of carbon ion therapy, previously only used in Europe and Japan. Further investigation into the link between physical and biological radiation effects and development of track-structure based radiation quantities is a key priority for the European Joint Programme for the Integration of Radiation Protection Research.

Potential future impact

The project developed the methodology for determining the weighting factors to convert an absorbed dose to a biological effective dose, and the multiscale approach has given a better understanding of the measurement techniques and how to characterise the beams. This will pave the way for the future development of radiation treatment planning tools. Optimised radiotherapy plans, in terms of physical dose and the predicted treatment outcome, will enable clinical radiotherapy plans from different radiotherapy centres in Europe to be compared. Since the number of patients treated at any given centre for a particular indication is often small, multi-centre studies will increase statistical power and improve utilisation of clinical data. The project may reduce the need for expensive radiobiological cell experiments, and reduce biological waste and animal experiments.

The future treatment planning tools will allow different radiotherapy modalities to be combined, providing radiotherapy researchers with improved capabilities based on sound metrological principles and dosage quantification. This will strongly support the realisation of the ESTRO 2020 Vision of individualised radiotherapy; and will have a wide impact on clinical practice and the radiotherapy technology industry. The project will contribute to increasing cure rates for the predicted 50 million European citizens that will be diagnosed with cancer and treated with radiotherapy over the next two decades, and reduce the side effects of cancer treatments and post-treatment patient care.

The concepts developed within the project could also be extended to a wider range of applications such as secondary cancer risks due to exposure of non-target regions in radiotherapy, health risks from low-dose environmental exposure (e.g. Radon gas), exposure of occupational radiation workers, accidental exposure and space radiation effects.

5 Website address and contact details

A public website (http://www.ptb.de/emrp/bioquart.html) has been created and maintained, where a general description of the project, the main deliverables, results have been made available for end users and the general public. The website also served to keep the interested public informed about project meetings and events.

The following persons can be contacted for questions about the project:

General questions about the project	Hans Rabus (PTB)	hans.rabus@ptb.de
Microdosimetric measurements	Sebastian Galer (NPL)	sebastian.galer@npl.co.uk
Nanodosimetric measurements	Gerhard Hilgers (PTB)	gerhard.hilgers@ptb.de
Reactive species measurements	Peter Sharpe (NPL)	peter.sharpe@npl.co.uk
Ion microbeams	Ulrich Giesen (PTB)	ulrich.giesen@ptb.de
γ-H2AX foci, DNA double strand breaks	Gaëtan Gruel (IRSN)	gaetan.gruel@irsn.fr
Chromosomal aberrations	Antonella Testa (ENEA)	antonella.testa@enea.it
Multi-scale modeling	Carmen Villagrasa (IRSN)	carmen.villagrasa@irsn.fr

Project Logo

List of all project participants
The following researchers have worked in the BioQuaRT project. Contact details are only given for those who were still with their affiliation at the end of the project life.

Name	Affiliation	email
Antonella Testa	ENEA	antonella.testa@enea.it
Massimo Pinto	ENEA	massimo.pinto@enea.it
Clarice Patrono	ENEA	clarice.patrono@enea.it
Sabina Chiriotti	SCK.CEN	scalvare@sckcen.be
Marcin Pietrzak	NCBJ	marcin.pietrzak@fuw.edu.pl
Joan Francesc Barquineiro Estruch	IRSN	
Sylvain Meylan	IRSN	sylvain.meylan@irsn.fr
Marta Bueno	IRSN	marta.buenovizcarra@irsn.fr
Davide Bianco	IRSN	
Gaëtan Gruel	IRSN	gaetan.gruel@irsn.fr
Pascale Voisin	IRSN	pascale.voisin@irsn.fr

Name	Affiliation	email
Carmen Villagrasa	IRSN	carmen.villagrasa@irsn.fr
Géraldine Gonon	IRSN	geraldine.gonon@yahoo.fr
Octávia Monteiro Gil	IST	ogil@ctn.ist.utl.pt
Pedro Teles	IST	ppteles@ctn.ist.utl.pt
Mónica Filipa dos Santos Mendes	IST	monicamendes@ctn.ist.utl.pt
Aliaksandr Bantsar	NCBJ	aliaksandr.bantsar@ncbj.gov.pl
Stan Pszona	NCBJ	pszona.stanislaw@ncbj.gov.pl
Jakub Bielecki	NCBJ	
Ling Hao	NPL	Ling.hao@npl.co.uk
Caterina Minelli	NPL	caterina.minelli@npl.co.uk
Kamran Fathi	NPL	kamran.fathi@npl.co.uk
David Cox	NPL	David.cox@npl.co.uk
John Gallop	NPL	John.gallop@npl.co.uk
Hugo Palmans	NPL	hugo.palmans@npl.co.uk
Peter Sharpe	NPL	peter.sharpe@npl.co.uk
Sebastian Galer	NPL	sebastian.galer@npl.co.uk
Giuseppe Schettino	NPL	giuseppe.schettino@npl.co.uk
David Crossley	NPL	david.crossley@npl.co.uk
Sam Flynn	NPL	Sam.flynn@npl.co.uk
Bo Li	NPL	bo.li@npl.co.uk
Davide Bortot	PoliMi	davide.bortot@polimi.it
Andrea Pola	PoliMi	andrea.pola@polimi.it
Marion Bug	PTB	marion.bug@ptb.de
Ticia Buhr	PTB	ticia.buhr@ptb.de
Alexander Arndt	PTB	alexander.arndt@ptb.de
Johannes Rahm	PTB	johannes.rahm@ptb.de
Mingjie Wang	PTB	mingjie.wang@ptb.de
Heidi Nettelbeck	PTB	heidi.nettelbeck@ptb.de
Daniel Bennett	PTB	daniel.bennett@ptb.de
Benedikt Rudek	PTB	benedikt.rudek@ptb.de
Gerhard Hilgers	PTB	gerhard.hilgers@ptb.de
Hans Rabus	PTB	hans.rabus@ptb.de
Ulrich Giesen	PTB	ulrich.giesen@ptb.de
Wolfgang Helms	PTB	wolfgang.helms@ptb.de
Frank Langner	PTB	frank.langner@ptb.de

Name	Affiliation	email
Woon Yong Baek	PTB	woonyong.baek@ptb.de
Thorsten Schneider	PTB	thorsten.schneider@ptb.de
Valeria Conte	INFN	valeria.conte@lnl.infn.it
Davide Moro	INFN	davide.moro@lnl.infn.it
Paolo Colautti	INFN	paolo.colautti@lnl.infn.it
Frauke Alexander	MRI	frauke.alexander@lrz.tum.de
Jan Wilkens	MRI	wilkens@tum.de
Ana Belchior	IST-ID	anabelchior@tecnico.ulisboa.pt

6 List of publications

Results of the BioQuaRT project have led or contributed to the following publications. Only papers which were published or accepted for publication by the time this report was issued are included here, a number of additional manuscripts is still under preparation.

[1] S. Pszona, B. Grosswendt, A. Bantsar, I. Cieszykowska, W. Czarnacki: *Nanodosimetry of ^{125}I – Auger electrons – Experiment and modeling.* Radiation Measurement 47, 1092-1096 (2012).

[2] W. Y. Baek, A. Arndt, M. U. Bug, H. Rabus, M. Wang: *Total electron scattering cross sections of pyrimidine.* Physical Review A 88, 032702 (2013). doi: dx.doi.org/10.1103/PhysRevA.88.032702

[3] M. U. Bug, E. Gargioni, H. Nettelbeck, W. Y. Baek, G. Hilgers, A. B. Rosenfeld, H. Rabus: *Ionization cross section data of nitrogen, methane, and propane for light ions and electrons and their suitability for use in track structure simulations.* Physical Review E 88, 043308 (2013). doi: 10.1103/PhysRevE.88.043308

[4] D. Moro, P. Colautti, V. Conte, G. Hilgers, A. Pausewang, W. Helms, B. Lambertsen, H. Rabus: *ILITS Experiment at TANDEM-ALPI accelerator.* INFN-LNL Report 239, 178-179 (2013).

[5] G. Hilgers, M. U. Bug, E. Gargioni, H. Rabus: *Comparison of measured and Monte-Carlo simulated track structure parameters in nanometric volumes.* Radiation Protection Dosimetry 161, 441-444 (2014). doi: 10.1093/rpd/nct265

[6] M. U. Bug, E. Gargioni, W. Y. Baek, G. Hilgers, H. Nettelbeck, H. Rabus: *Proton-impact ionization cross sections for nanodosimetric track structure simulations.* Radiation Protection Dosimetry 161, 474-477 (2014). doi: dx.doi.org/10.1093/rpd/nct317

[7] D. Moro, S. Chiriotti, P. Colautti and V. Conte: *TEPC gas gain measurements in propane.* Radiation Protection Dosimetry 161, 459-463 (2014). doi: 10.1093/rpd/ncu005

[8] Aliaksandr Bantsar, Marcin Pietrzak, Marian Jaskóła, Andrzej Korman, Stanisław Pszona, Zygmunt Szefliński: *Status report: Nanodosimetry of carbon ion beam at HIL.* Reports of Practical Oncology & Radiotherapy 19, S42-S46 (2014).

[9] G. Hilgers, W. Helms, B. Lambertsen, A. Pausewang, H. Rabus, A. Bantsar, S. Pszona, Z. Szeflinski: *ILITS Experiment: First Results.* HIL Annual Report 2013, 46-48 (2014).

[10] G. Hilgers, D. Moro, A. Pausewang, W. Helms, B. Lambertsen, H. Rabus, P. Colautti, V. Conte: *ILITS Experiment: First Results.* INFN-LNL Report 240, 129-130 (2014).

[11] D. Bianco, C. Villagrasa and M. Dos Santos: *Multi-Scale Analysis of Simulated Proton and Alpha Irradiation.* Radiation Protection Dosimetry 164, 444-448 (2014). doi: 10.1093/rpd/ncu187

[12] W. Y. Baek, M. U. Bug, H. Rabus: *Differential elastic electron scattering cross sections of pyrimidine in the energy range between 20 eV and 1 keV.* Physical Review A 89, 062716 (2014). doi: 10.1140/epjd/e2014-40829-8

[13] C. Champion, M. A. Quinto, M. U. Bug, W. Y. Baek and P. F. Weck: *Theoretical and experimental quantification of doubly and singly differential cross sections for electron-induced ionization of isolated tetrahydrofuran molecules.* European Physics Journal D, 68: 205, 1-7 (2014). doi: 10.1140/epjd/e2015-60095-6

[14] Marion U. Bug, Gerhard Hilgers, Woon Yong Baek, Hans Rabus: *Nanodosimetric characterization of ion beams.* European Physics Journal D 68: 217, 1-10 (2014). doi: 10.1140/epjd/e2014-50015-9

[15] H. Rabus, H. Palmans, G. Hilgers, P. Sharpe, M. Pinto, C. Villagrasa, H. Nettelbeck, D. Moro, A. Pola, S. Pszona, P. Teles: *Biologically Weighted Quantities in Radiotherapy: an EMRP Joint Research Project.* EPJ Web of Conferences 77: 00021, 1-7 (2014); doi: 10.1051/epjconf/20147700021

[16] H. Palmans, H. Rabus, A. L. Belchior, M. U. Bug, S. Galer, U. Giesen, G. Gonon, G. Gruel, G. Hilgers, D. Moro, H. Nettelbeck, M. Pinto, A. Pola, S. Pszona, G. Schettino, P. H. G. Sharpe, P. Teles, C. Villagrasa and J. J. Wilkens: *Future development of biologically relevant dosimetry.* British Journal of Radiology 88:20140392, 1-19 (2015). doi: 10.1259/bjr.20140392

[17] Marion Bug: *Nanodosimetric Particle Track Simulations in Water and DNA Media.* University of Wollongong, Wollongong, NSW, Australia 13 November 2014, http://ro.uow.edu.au/theses/4150/

[18] A. Arndt, W. Y. Baek, M. U. Bug, T. Buhr, G. Hilgers, H. Nettelbeck, H. Rabus, J. Rahm, M. Wang: *Progress Report of the Department 'Fundamentals of Dosimetry'.* Report CCRI(I)/13-10, 29-41 (2015). http://www.bipm.org/cc/CCRI(I)/Allowed/21/CCRI(I)_ProgressReport_PTB_2013.pdf

[19] C. Patrono, O. Monteiro Gil, U. Giesen, F. Langner, M.Pinto, H. Rabus, A. Testa: *"BioQuaRT" project: design of a novel in situ protocol for the simultaneous visualization of chromosomal aberration and micronuclei after irradiation at microbeam facilities.* Radiation Protection Dosimetry 166, 197-199 (2015). doi: 10.1093/rpd/ncv160

[20] D. Moro, S. Chiriotti, V. Conte, P. Colautti and B. Grosswendt: *Lineal energy calibration of a spherical TEPC.* Radiation Protection Dosimetry 166, 233-237 (2015), doi: 10.1093/rpd/ncv153

[21] S. Chiriotti, D. Moro, V. Conte, P. Colautti, B. Grosswendt, E. Sterpin, S. Vynckier: *Influence of the Physical Data to Calibrate TEPCs.* Radiation Protection Dosimetry 166, 238-241 (2015). doi: 10.1093/rpd/ncv140

[22] A. Bantsar, G. Hilgers, S. Pszona, H. Rabus and Z. Szeflinski: *Experimental investigation of ionization track structure of carbon ions - experiments at HIL Warsaw.* Radiation Protection Dosimetry 166, 253-256 (2015). doi: 10.1093/rpd/ncv191

[23] Thorsten Schneider, Hans Rabus, Marion U. Bug: *A database application to investigate the validity of the nanodosimetric approach.* Radiotherapy & Oncology 115 (Suppl. 1), S734-S735 (2015). doi: 10.1016/S0167-8140(15)41355-6

[24] Hans Rabus: *Requirements for multi-scale models of radiation action – activities in European projects Nano-IBCT and BioQuaRT.* Radiotherapy & Oncology Oncology 115 (Suppl. 1), S107 (2015). doi: 10.1016/S0167-8140(15)40210-5

[25] Marion U. Bug, Woon Yong Baek, Hans Rabus: *Calculation of electron track structure in water and DNA medium.* Radiotherapy & Oncology 115 (Suppl. 1), S76 (2015).doi: 10.1016/S0167-8140(15)40154-9

[26] C. Villagrasa, G. Gruel, G. Gonon, S. Meylan, M. Bug, U. Giesen, M. Bueno, W. Y. Baek, A. Arndt, H. Rabus: *Characterisation of interaction of radiation with cells- track structure modelling and biodescriptors of the topology of energy deposition.* Radiotherapy & Oncology 115 (Suppl. 1), S106-S107 (2015). doi: 10.1016/S0167-8140(15)40209-9

[27] D. Moro: *Experimental methods for microdosimetry, nanodosimetry and track structure determination: state of the art.* Radiotherapy & Oncology 115 (Suppl. 1), S106-S107 (2015). doi: 10.1016/S0167-8140(15)40208-7

[28] F. Alexander, C. Villagrasa, H. Rabus, J.J. Wilkens: *Exploring the potential of nanometric track structure based quantities for particle beam treatment planning.* Radiotherapy & Oncology 115 (Suppl. 1), S796 (2015). doi: 10.1016/S0167-8140(15)41460-4

[29] U. Kamierczak, A. Bantsar, D. Banas, J. Braziewicz, J. Czub, M. Jaskóla, A. Korman, M. Kruszewski, A. Lankoff, H. Lisowska, M. Pietrzak, S. Pszona, T. Stepkowski, Z. Szeflinski, M. Wojewódzka: *Heavy Ion Beams for Radiobiology: Dosimetry and Nanodosimetry at HIL.* Acta Physica Polonica A 127, 1516-1519 (2015). doi: 10.12693/APhysPolA.127.1516

[30] A.Bantsar, S.Pszona: *Nanodosimetry of Electons: Analysis by Experiment and Modelling.* Radiation Protection Dosimetry 166, 210-213 (2015). doi: 10.1093/rpd/ncv301

[31] S. Chiriotti, D. Moro, P. Colautti, V. Conte, B. Grosswendt: *Equivalence of Pure Propane and Propane TE Gases for Microdosimetric Measurements.* Radiation Protection Dosimetry 166, 238-241 (2015). doi: 10.1093/rpd/ncv293

[32] G. Hilgers, D. Moro, A. Pausewang, W. Helms, B. Lambertsen, H. Rabus, P. Colautti, V. Conte: *ILITS experiment: track structure of carbon ions.* INFN-LNL Report 241, 132-133 (2015)

[33] S. Chiriotti, D. Moro, E. Motisi, M. Ciocca, P. Colautti, V. Conte, B.Grosswendt. : *First Microdosimetric Measurements at CNAO.* INFN-LNL Report 241, 141-142 (2015)

[34] V. Conte, D. Moro, P. Colautti, B. Grosswendt, G. Hilgers and H. Rabus: *The Ion Counter and the StarTrack Counter: consistent nanodosimetry of track structure for carbon ions.* INFN-LNL Report 241, 164-165 (2015)

[35] G. Hilgers, W. Helms, B. Lambertsen, A. Pausewang, H. Rabus, A. Bantsar, S. Pszona, Z. Szeflinski: *ILITS experiment: scaling of cluster size distributions.* HIL Annual Report 2014, 48-51 (2015)

[36] M. Pietrzak, A. Bantsar and S. Pszona: *Nanodosimetry of Carbon Ions at HIL - study of the wall effect in the Jet Counter.* HIL Annual Report 2014, 54-56 (2015)

[37] A. Bantsar, G. Hilgers, M. Pietrzak, S. Pszona and H. Rabus: *Nanodosimetry of carbon ions - comparison of the experiments with Ion Counter and Jet Counter.* NCBJ Annual Report 2014, 59 (2015)

[38] F. Alexander, C. Villagrasa, H. Rabus J. Wilkens: *Energy dependent track structure parametrisations for protons and carbon ions based on nanometric simulations.* European Physics Journal D 69:237, 1-7 (2015). doi: 10.1140/epjd/e2015-60206-5

[39] B. Rudek, D. Bennett, M. Wang, A. Arndt, H. Rabus: *Ion induced fragmentation cross-sections of DNA constituents.* European Physics Journal D 69:237, 1-9 (2015). doi: 10.1140/epjd/e2015-60204-7

[40] G. Hilgers, M. U. Bug, E. Gargioni, H. Rabus: *Effect of secondary ionizations on the comparison of measured and simulated track structure parameters in nanometric volumes.* European Physics Journal D 69:239, 1-18 (2015). doi: 10.1140/epjd/e2015-60176-6

[41] F. Alexander, C. Villagrasa, H. Rabus, J. J. Wilkens: *Local weighting of nanometric track structure properties in macroscopic voxel geometries for particle beam treatment planning.* Physics in Medicine and Biology 60, 9145-9156 (2016), doi: 10.1088/0031-9155/60/23/9145

[42] S. Chiriotti, D. Moro, V. Conte, B. Grosswendt, F. Vanhavere and S. Vynckier: *Indirect method to monitor the site size of sealed spherical TEPCs.* Radiation Measurements 85, 26-31 (2016),

[43] M. Wang, B. Rudek, T. Buhr, D. Bennett, M. Bug, P. de Vera, W. Y. Baek, G. Hilgers and H. Rabus: *Cross sections for ionization of tetrahydrofuran by protons at energies between 300 and 3000 keV.* Physical Review A 93, 052711, 1-16 (2016). doi: 10.1103/PhysRevA.93.052711

[44] B. Rudek, D. Bennett, M. Bug, M. Wang, W. Y. Baek, T. Buhr, G. Hilgers, C. Champion, H. Rabus: *Double differential cross sections for proton induced electron emission from molecular analogues of DNA constituents for energies in the Bragg peak region.* The Journal of Chemical Physics, 145, 104301, 1-12 (2016), doi: 10.1063/1.4962171

[45] M. Bug, W. Y. Baek, H. Rabus, C. Villagrasa, S. Meylan, A. B Rosenfeld: *An electron-impact cross section data set (10 eV - 1 keV) of DNA constituents based on consistent experimental data: a requisite for Monte Carlo simulations.* Radiation Physics and Chemistry 130, 459–479 (2017), doi: 10.1016/j.radphyschem.2016.09.027